D. G. Truhlar, F. B. Brown, R. Steckler, and A. D. Isaacson, in *The Theory of Chemical Reaction Dynamics*, edited by D. C. Clary (D. Reidel, Dordrecht, Holland, 1986), pp. 285-329.

or: D. G. Truhlar, F. B. Brown, R. Steckler, and A. D. Isaacson, NATO ASI Ser. C **170**, 285-329 (1986).

THE REPRESENTATION AND USE OF POTENTIAL ENERGY SURFACES IN THE WIDE VICINITY OF A REACTION PATH FOR DYNAMICS CALCULATIONS ON POLYATOMIC REACTIONS

Donald G. Truhlar, Franklin B. Brown, and Rozeanne Steckler
Department of Chemistry
University of Minnesota
Minneapolis, Minnesota 55455

and Alan D. Isaacson
Department of Chemistry
Miami University
Oxford, Ohio 45056

ABSTRACT. We consider three aspects of potential energy surface representations for dynamics calculations on polyatomic systems, with special emphasis on generalized transition state theory and tunneling calculations. (i) We present methods for calculating the vibrational energies of generalized transition states from either a cartesian or internal-coordinate force field and including the effect of mode-mode couplings on the rate constant by perturbation theory and the Pitzer-Gwinn approximation. (ii) We discuss practical aspects in the use of ab initio gradient-based electronic structure calculations for the calculation of cartesian force fields for a set of stationary points on the potential energy surface or for a sequence of generalized transition states. (iii) We discuss recent progress on the development of global analytic representations for potential energy surfaces of polyatomic reactions. Such global representations can be used to generate either cartesian or internal-coordinate force fields for generalized transition states, and they can also be used to compute the potential energy surface far from the minimum energy path as may be required for tunneling calculations in some cases.

1. INTRODUCTION

The calculation of reaction rates is generally carried out in two steps. In the first step one calculates or models the potential energy surface,[1,2] PES (or surfaces; however in the present report we limit our attention to electronically adiabatic reactions for which only a single surface is involved). In the second step one calculates dynamical quantities, using the PES as given.[1,3] It is becoming increasingly clear, however, that these two steps should not be performed independently. In the first place, the dynamics calculations are expected to be more sensitive to some features of the PES than to others, and it would be desirable (in the practical case where the PES is not equally accurate

D. C. Clary (ed.), The Theory of Chemical Reaction Dynamics, 285–329.

for all possible geometries) to expend the greatest fraction of the theoretical effort on those features of the PES that are expected to have the greatest effect on the dynamical results of interest.[4] In the second place, when the PES is based on ab initio electronic structure calculations it is not practical economically to perform calculations for all possible geometries of the reacting molecule or molecules. The disparity between the number of calculations needed to map a reasonable grid of all relevant geometrical parameters and the number of affordable calculations grows rapidly with the number N of atoms involved. To span each internal coordinate with only 10 points already requires 10^{3N-6} geometries to be considered, which is unaffordable for $N \geq 4$. Of course an accurate PES is not needed at all possible geometries, and thus, when using the ab initio approach, we want to calculate--and fit or represent --the potential only where it is really important.

One approach to circumvent the problems mentioned above is to combine a local representation of the PES in the vicinity of the reaction path with dynamics calculations based on localized bottlenecks and localized semiclassical tunneling paths. A large amount of experience has been gained with these methods[5-10] for reactions with only a few atoms. In our group we have made extensive tests of the reliability of such methods by comparing the results to those from accurate quantal dynamics calculations for simple systems and to experiment. On the basis of these tests we can conclude that methods based on localized dynamical bottlenecks and localized semiclassical tunneling paths are capable of accurate predictions of thermal and some state-selected reaction rates, kinetic isotope effects, and threshold energies for overall reaction[9-22] and sometimes for reaction into specific product vibrational states,[19,23,24] as well as predictions of resonance energies and lifetimes and branching ratios for decay[25-29] and spectroscopic tunneling splittings.[30] Reaction path methods have also been applied to treat energy transfer in nonreactive processes.[31-33] Methods based on an expansion in reaction-path coordinates about the minimum-energy path are sometimes called reaction-path Hamiltonian (RPH) methods,[8,27,28,34-36] although the idea is older than the name.[37-39] The emphasis in much RPH research is on a correct formulation of the kinetic energy in reaction-path coordinates.[34,35,40] In the present paper, however, we wish to emphasize the representation of the potentials, especially for systems with four or more atoms. We also wish to emphasize that in many cases the PES must be known in regions beyond those where it can be predicted by a quadratic or other expansion about the minimum-energy path, e.g., even in regions where reaction-path coordinates are not unique.[15,18-22] These wider regions are still localized though and can be identified with reasonable confidence so that we do not need a complete global representation of the PES.

There are two reasons why one needs to go beyond a quadratic expansion about the minimum-energy path. The first is anharmonicity, which may be especially important for low-frequency modes, and which is essential for even a qualitatively correct treatment of bifurcating reaction paths. It is also very important for quantitative calculations of low-temperature rate constants to include anharmonicity of high-frequency modes. The second is tunneling in systems with intermediate and large

curvature of the reaction path. In such systems the best semiclassical tunneling paths may be very far from the reaction path. In such regions reaction-path coordinates can become multivalued, making the RPH kinetic energy operator invalid. To treat such regions we transform locally to mass-scaled cartesians, which are valid everywhere. For systems with large reaction-path curvature [for short, we call these large-curvature (LC) systems], the region over which we require the potential may be envisioned as a multidimensional tube surrounding the minimum-energy path and including extra wide regions for possible tunneling paths on the concave sides of elbows. It is convenient to call this extended region around the reaction path the reaction swath, and we arrive at the reaction-swath potential (RSP) as an intermediate construct, or level of required knowledge, between the RPH on one hand and the global PES on the other.

Two quantities which play a primary role in the use of an RPH for dynamics calculations are the generalized free energy of activation curves $\Delta G_T^{GT,O}(s)$ and the vibrationally adiabatic potential curves $V_a^g(n_i,s)$. The former are used for variational transition state theory (VTST) calculations of thermal reaction rates with classical reaction-coordinate motion, and the latter are used for calculating overall and state-specific threshold energies, tunneling probabilities, and the properties of resonance states. Section 2 reviews the basic definitions of these quantities and also reviews the independent-normal-mode (INM) approximation that provides the simplest way to actually calculate $\Delta G_T^{GT,O}(s)$ and $V_a^g(n_i,s)$ for polyatomic systems. The INM approximation may be implemented harmonically or anharmonically but it includes only principal force constants† in normal coordinates. Then we discuss a better method to treat anharmonicity by first modelling the potential energy in curvilinear internal coordinates and then transforming it to a normal coordinate representation. The motivations for this approach are presented, and the practical procedures necessary for calculations are outlined in detail.

Section 2 also includes a brief review of the large-curvature and least-action tunneling approximations with emphasis on delineating the regions of the PES required for such calculations.

Sections 3 and 4 are concerned with the representation of the potential energy information that is needed as input for the calculations of Section 2. In particular, to carry out the calculations of Section 2 we must be able to generate the PES at any point near the reaction path for small-curvature (SC) systems and at any point in the reaction swath, as defined above, for LC systems.

Section 3 discusses ab initio calculations of the RPH by so-called "gradient methods", which are algorithms for the direct calculation of

†We use the convention, from spectroscopy, that "principal" force constants describe the potential within a single normal or internal-coordinate mode whereas "interaction" force constants describe mode-mode coupling. This convention avoids confusion with "diagonal" and "off-diagonal" matrix elements in a perturbation theory treatment of anharmonicity.

PES derivatives. Gradient techniques are better suited to calculating expansions about the reaction path than to calculating the full RSP, and we will limit this initial discussion to the RPH. In a calculation based on ab initio gradient methods, the potential may conveniently be represented in terms of a finite number of force constant matrices, each corresponding to an expansion about a different point on or near the minimum-energy path. This obviates the need for choosing specific functional forms, but it raises a number of new questions about computational economics and step sizes. These will be discussed and simulated gradient calculations based on global PES's will be presented to demonstrate some practical difficulties.

Section 4 discusses methods of representing the PES, or at least the full RSP, in terms of globally defined functional forms. This section begins with a review of methods for fitting atom-diatom PES's and methods developed previously for representing polyatomic PES's. Then we discuss a new approach. The most important elements in the new approach are that the globally defined functional form is required to be accurate only in the reaction swath, and it is flexibilized in this swath by making globally significant potential parameters explicit functions of selected coordinates. Illustrative examples and possible pitfalls are also included.

2. DYNAMICAL CALCULATIONS

2.1. Variational Transition State Theory, Vibrationally Adiabatic Potential Curves, and Tunneling

In canonical variational transition state theory (CVTST or, for short, CVT) the rate constant for a temperature T is calculated in three steps. First one calculates the hybrid generalized transition state theory (GTST or, for short, GT) rate constant $k^{GT}(T,S^{GT})$ as a function of the location S^{GT} of the generalized transition state.[9,41-44] The word "hybrid" here refers to the fact that in this calculation the reaction coordinate is treated classically but all other degrees of freedom are quantized, and the word "generalized" refers to the fact that the generalized transition state is not required to pass through the saddle point as in conventional[45] transition state theory. In the second step one minimizes $k^{GT}(T,S^{GT})$ with respect to S^{GT} yielding the hybrid CVT rate constant[9,41-44]

$$k^{CVT}(T) = \min_{S^{GT}} k^{GT}(T,S^{GT}) \quad . \tag{1}$$

The words "canonical" and "variational" in CVT refer to the fact that in this step the dividing surface is variationally optimized for the canonical ensemble specified by T. In the third step one multiplies $k^{CVT}(T)$ by a transmission coefficient $\kappa(T)$ to account for quantal effects on the reaction coordinate, yielding the final estimated rate constant:[9,42-44]

$$k^{CVT/\kappa}(T) = \kappa(T)\, k^{CVT}(T) \ . \qquad (2)$$

In principle the generalized transition state can be any hypersurface in phase space except for the constraint that it must divide reactants from products.[46] However, in practice it would be difficult to calculate $k^{GT}(T,S^{GT})$ for arbitrary dividing surfaces as well as to perform the variational step of eq. (1) for all possible surfaces. To make VTST practical one must define a subset of all possible dividing surfaces for which these steps are realizable and yet which is capable of yielding the required accuracy. It is our contention, based on extensive computational experience, that such a subset is provided by a one-parameter sequence of surfaces perpendicular to a physically chosen reference path that leads from reactants to products. In most cases this reference path is chosen to be the minimum-energy path through mass-scaled or mass-weighted cartesians.[38,47-50†] Here we call this path the MEP; sometimes it is called the intrinsic reaction coordinate (IRC). The distance along the MEP from a reference point (which is usually defined as the highest saddle point if there is one) is called the reaction coordinate s, and the dividing surfaces are parametrized by the value of s at which they intersect the MEP. In the vicinity of their intersection with the MEP, the dividing surfaces are taken to be hyperplanes in the mass-scaled cartesian space that are perpendicular to the MEP; more globally they are bent if necessary to insure that they separate reactants from products.

The hybrid GTST rate constant for the generalized transition state at s is[42-44]

$$k^{GT}(T,s) = (\tilde{k}T/h)K^{\ddagger,0}\exp[-\Delta G_T^{GT,0}(s)/\tilde{k}T] \qquad (3)$$

where $\tilde{k}$ is Boltzmann's constant, h is Planck's constant, $K^{\ddagger,0}$ is unity for unimolecular reactions and the reciprocal of the standard-state concentration for bimolecular reactions, and $\Delta G_T^{GT,0}(s)$ is the generalized standard-state free energy of activation. The subscript on $\Delta G_T^{GT,0}(s)$ denotes the temperature. The generalized free energy of activation is expressed as[51]

$$\Delta G_T^{GT,0}(s) = -\tilde{k}T \ln [K_{eq}^{GT}(T,s)/K^{\ddagger,0}] \qquad (4)$$

where $K_{eq}^{GT}(T,s)$ is a quasiequilibrium constant for forming generalized

---

†In mass-scaled cartesians the three cartesian coordinates of atom A are scaled by $(m_A/\mu)^{\frac{1}{2}}$ where m_A is the mass of A and μ is an arbitrary convenient mass. In mass-weighted cartesians the coordinates of atom A are weighted by $m_A^{\frac{1}{2}}$. Mass-scaled coordinates have units of length; mass-weighted coordinates have units of mass$^{\frac{1}{2}}$ length, and are usually given as $u^{\frac{1}{2}}$ Å or $u^{\frac{1}{2}}$ a_0, where 1 u = 1 universal (^{12}C) atomic mass unit = 1822.887 m_e, and 1 a_0 = 1 bohr = 0.5291771 Å.

transition states from reactants. For a unimolecular reaction

$$K_{eq}^{GT}(T,s) = \frac{Q^{GT}(T,s)}{Q^{R}(T)} \exp[-V_{MEP}(s)/\tilde{k}T] \tag{5}$$

and for a bimolecular one

$$K_{eq}^{GT}(T,s) = \frac{Q^{GT}(T,s)}{\Phi^{R}(T)} \exp[-V_{MEP}(s)/\tilde{k}T] \tag{6}$$

where $Q^{GT}(T,s)$ and $Q^{R}(T)$ are the partition functions for the generalized transition state and reactants, respectively, $\Phi^{R}(T)$ is $Q^{R}(T)$ per unit volume, and $V_{MEP}(s)$ is the Born-Oppenheimer potential at the point where the generalized transition state intersects the MEP.

In eqs. (5) and (6) the zero of energy for $V_{MEP}(s)$, $Q^{R}(T)$, and $\Phi^{R}(T)$ is at the equilibrium geometry of reactants, and the zero of energy for $Q^{GT}(T,s)$ is $V_{MEP}(s)$. It is also very popular to define partition functions with respect to the local zero point energy. For this purpose we define

$$V_{a}^{G}(s) = V_{MEP}(s) + \varepsilon^{G}(s) \tag{7}$$

and

$$\Delta V_{a}^{G}(s) = V_{a}^{G}(s) - \varepsilon^{RG} \tag{8}$$

where $\varepsilon^{G}(s)$ is the zero point energy at s, and ε^{RG} is the zero point energy of reactants. [$\Delta V_{a}^{G}(s)$ is called the ground-state adiabatic potential curve.] Then eqs. (5) and (6) become

$$K_{eq}^{GT}(T,s) = \frac{\tilde{Q}^{GT}(T,s)}{\tilde{Q}^{R}(T) \text{ or } \tilde{\Phi}^{R}(T)} \exp[-\Delta V_{a}^{G}(s)/\tilde{k}T] \tag{9}$$

where, for example,

$$\tilde{Q}^{GT}(T,s) = Q^{GT}(T,s) \exp[\varepsilon^{G}(s)/\tilde{k}T] \tag{10a}$$

$$= \sum_{\alpha} d_{\alpha} \exp\{-[\varepsilon(\alpha,s) - \varepsilon^{G}(s)]/\tilde{k}T\} . \tag{10b}$$

In eq. (10b), $\varepsilon(\alpha,s)$ is the energy of level α of the generalized transition state and d_{α} is the degeneracy of level α.

In calculating $Q^{GT}(T,s)$, we fix the system in a hypersurface orthogonal to the reaction path at a fixed value of s. This is equivalent to an adiabatic approximation with all generalized-transition-state modes treated as adjusting adiabatically to changes in s. The usual

approximation is to further assume that $\epsilon(\alpha,s)$ is a sum of electronic, vibrational, and rotational energies. The vibrational modes may be additionally decoupled from each other by the harmonic adiabatic approximation but are coupled nonadiabatically in the kinetic energy operator and anharmonically by the potential. The kinetic coupling element for modes k and k' is denoted by $\mathcal{B}_{kk'}(s)$ and it arises from the twisting of the normal modes around the MEP and into each other. Each element $\mathcal{B}_{kk'}(s)$ is the scalar product of the generalized normal mode vector for mode k' and the derivative of the generalized normal mode vector for mode k with respect to the reaction coordinate at s. Since the MEP is curved, there are also coupling elements between the generalized normal mode motions and motion along the reaction coordinate. These elements are called $\mathcal{B}_{kF}(s)$, where F indexes the reaction coordinate and there are F-1 generalized normal modes (F = 3N-5 or 3N-6 for N-atom generalized transition states that are linear or nonlinear, respectively). Each term $\mathcal{B}_{kF}(s)$ can be written in terms of the scalar product of the generalized normal mode vector of vibration k and the derivative of the gradient (representing motion along the reaction path) with respect to the reaction coordinate at s.

So far we have outlined the CVT formalism for calculating thermal reaction rates. In our CVT calculations we have neglected the nonadiabatic coupling elements, in which case CVT calculations require only the potential energy along the MEP and the energy levels for a sequence of generalized transition states. Transmission coefficients in the small-curvature semiclassical adiabatic (SCSA) approximation[10,52,53] depend on these same quantities plus the $\mathcal{B}_{kF}(s)$ curvature elements. Several other interesting reaction attributes may also be calculated from $V_{MEP}(s)$, $\epsilon(\alpha,s)$, and $\mathcal{B}_{kF}(s)$. For example, for interpretative purposes we are often interested in the location of the variationally optimized dividing surface; this is called the canonical variational transition state, and it is located at the maximum of $\Delta G_T^{GT,0}(s)$. The overall translational threshold energy in the absence of tunneling is given in the VTST approximation by the maximum of $\Delta V_a^G(s)$. Threshold energies for reactant or product molecules with a specific vibrational quantum number n for some high-frequency mode are sometimes given by the maxima of

$$V_a^g(n,s) = V_{MEP}(s) + \epsilon^g(n_i,s) \tag{11}$$

where $\epsilon^g(n_i,s)$ is the energy of the level of the generalized transition state that has quantum number n_i for the mode, i, that correlates to the specific reactant or product mode and quantum number 0 for all other modes. (The superscript g denotes the system is in the ground state for all modes whose quantum numbers are not explicitly specified whereas G denotes ground state for all modes.) Resonance energies are sometimes given by the energy levels of $V_a^g(s)$, and this quantity also sometimes serves as an effective potential for tunneling. Resonance decay probabilities depend on the $\mathcal{B}_{kF}(s)$ as well.

When the canonical variational transition state is strongly dependent on temperature, a more consistent theory is provided by improved canonical variational transition state theory (ICVTST or, for short,

ICVT).[44] As for the quantities discussed in the last paragraph, the ICVT approximation to the thermal rate constant may be calculated from $V_{MEP}(s)$ and the set of $\varepsilon(\alpha,s)$.

We mentioned in Sect. 1 that for LC systems the semiclassical tunneling paths may pass through regions where the RPH breaks down. We originally proposed two somewhat complicated schemes for calculating the tunneling probabilities in LC systems,[20,21] but later work[22] showed that almost identical results could be obtained with a simpler prescription for the tunneling paths. The approximation incorporating this simpler prescription is called the large-curvature approximation, version 3, or LC3.[54] In this approximation the semiclassical tunneling paths are straight lines through mass-scaled coordinates from an adiabatic translational turning point on the MEP in the entrance channel to a translational turning point on the MEP in the exit channel. For ground-state reactants or products the adiabatic translational turning points are defined as the points where an energy parameter $\tilde{E}$ equals $V_a^G(s)$; for excited states they are computed from $V_a^g(n_i,s)$ or its generalization. The energy parameter takes on all values from ε^{RG} to the total energy. The region of coordinate space between the LC3 path at the lowest total energy for which tunneling must be considered and the region where a quadratic expansion about the MEP is valid is included in the reaction swath; clearly the swath becomes wider when lower-energy tunneling processes must be considered.

For intermediate reaction-path curvature, one may use either the SCSA or LC3 approximation, but even more accurate results are obtained by a least-action (LA) method.[22,54] In the LA method, the tunneling paths are linear interpolations between the MEP and the LC3 paths. Thus this method does not require knowing the potential over a wider swath than is necessary for the LC3 method.

Babamov and Marcus[55] have proposed tunneling models in which the tunneling paths correspond to a fixed hyper-radius, where the hyper-radius is the distance from the origin in mass-scaled hyperspherical coordinates. These require a knowledge of the potential over about the same swath as required for LC3 calculations.

2.2. Independent-Normal-Mode Approximation

It should be clear from Sect. 2.1 that the generalized-transition-state energy levels $\varepsilon(\alpha,s)$ play a central role in VTST and related theories. Usually one writes $\varepsilon(\alpha,s)$ as a sum of electronic, vibrational, and rotational energies, in which case the partition functions become products of electronic, vibrational, and rotational factors. The electronic problem is often well approximated by assuming that reaction occurs with appreciable probability only on a single potential energy surface, and the rotational problem is usually treated accurately enough by simple classical approximations. The vibrational energies, $\varepsilon_{vib}(n_1,\ldots,n_{F-1},s)$, where n_m is a vibrational quantum number, and vibrational partition functions, $Q^{GT}_{vib}(T,s)$, however, are not obtained as straightforwardly, at least if one desires high accuracy.

In many respects the vibrations of generalized transition states are like those of ordinary molecules, and thus the generalized-

transition-state vibrational partition function $Q^{GT}_{vib}(T,s)$ may be calculated by many statistical methods developed for ordinary molecules (see Ref. 54 and references therein). One important distinction between a generalized transition state and an ordinary molecule, though, is that the former, being a hypersurface orthogonal to the reaction path, is missing one vibrational degree of freedom, which corresponds to the reaction-coordinate motion. To account for this we must calculate $\varepsilon_{vib}(n_1,\ldots,n_{F-1},s)$ and $Q^{GT}_{vib}(T,s)$ in the (F-1)-dimensional subspace that is orthogonal not only to overall translations and rotations, as for a real molecule, but also to the reaction path. To accomplish the dimensionality reduction we use the projection operator method of Miller et al.[34] In this method the harmonic frequencies and corresponding generalized normal modes are determined by diagonalizing the projected force constant matrix $\underset{\approx}{F}^P(s)$. This matrix is related to the force constant matrix $\underset{\approx}{F}(s)$, defined as the matrix of second derivatives of the potential energy with respect to mass-scaled cartesians, by[34,35]

$$\underset{\approx}{F}^P(s) = [\underset{\approx}{1} - \underset{\approx}{P}(s)]\underset{\approx}{F}(s)[\underset{\approx}{1} - \underset{\approx}{P}(s)] \tag{12}$$

where $\underset{\approx}{1}$ is the unit matrix and $\underset{\approx}{P}(s)$ is the projector which projects onto the mode directions corresponding to the three overall translations, the two or three rotations, and the motion along the reaction path. Thus, diagonalizing $\underset{\approx}{F}^P$ will yield 6 or 7 zero eigenvalues corresponding to the projected motions and 3N-6 or 3N-7 generalized normal mode frequencies which correspond to the vibrations orthogonal to the reaction path.

The simplest approach to treating the bound vibrational motions, in terms of both the computational effort and the amount of information required about the PES, is the harmonic approximation, under which the vibrational energy levels are given by

$$\varepsilon_{vib}(n_1,n_2,\ldots,n_{F-1},s) = \sum_{m=1}^{F-1} (n_m + \tfrac{1}{2})hc\bar{\nu}_m(s) \tag{13}$$

where n_m and $\bar{\nu}_m(s)$ are the vibrational quantum number and frequency in cm^{-1} for mode m, respectively, c is the speed of light in cm per unit time, and the energy is measured from the bottom of the vibrational well. The vibrational partition function,

$$Q^{GT}_{vib}(T,s) = \sum_{n_1,n_2,\ldots,n_{F-1}} \exp[-\beta\varepsilon_{vib}(n_1,n_2,\ldots,n_{F-1},s)] \tag{14}$$

where $\beta \equiv (\tilde{k}T)^{-1}$, is thus separable in the harmonic approximation and equals

$$Q^{GT}_{vib}(T,s) = \prod_{m=1}^{F-1} Q^{GT}_{vib,m}(T,s) \tag{15}$$

where the vibrational partition function for mode m is given by

$$Q^{GT}_{vib,m}(T,s) = \sum_{n_m} \exp[-\beta\epsilon_{vib,m}(n_m,s)] \qquad (16)$$

with $\epsilon_{vib,m}(n_m,s) = (n_m + \frac{1}{2})hc\bar{\nu}_m(s)$ in the harmonic approximation. The summation in eq. (16) should be terminated with the last term for which $\epsilon_{vib,m}(n_m,s)$ is less than $D-V_{MEP}(s)$, where D is the lowest dissociation energy of the system.[51,56] However, assuming that the contributions from energy levels above $D-V_{MEP}(s)$ are negligible for the temperature being considered and extending the summation in eq. (16) over all harmonic levels, it can be summed analytically to yield

$$Q^{GT}_{vib,m}(T,s) = \exp[-hc\bar{\nu}_m(s)\beta/2]\{1 - \exp[-hc\bar{\nu}_m(s)\beta]\}^{-1} \ . \qquad (17)$$

Since, in general, the vibrational degrees of freedom are anharmonic, substantial errors can be obtained in CVT rate constants computed under the harmonic approximation.[43,57-59] As an example of the effect of including anharmonicity in the calculation of quantal CVT rate constants, we consider the reaction $OH + H_2 \rightarrow H_2O + H$, which has been studied[59] using the analytic PES obtained by Schatz and Elgersma[60] by a fit to the ab initio calculations of Walch and Dunning.[61] For this reaction, the CVT/SCSAG rate constants obtained with the harmonic approximation for the bound vibrational motions were found to overestimate the best anharmonic results [obtained within the independent-normal-mode (INM) framework described below] by factors of 2.27 at 298 K and 1.32 at 2400 K. [Note: The G at the end of SCSAG or other tunneling method abbreviations denotes that $\kappa(T)$ is based on ground-state tunneling probabilities.]

One practical approach to the inclusion of vibrational anharmonicity is to neglect the mode-mode coupling of the normal modes and to employ an approximate anharmonic potential curve to describe the motion along each generalized normal mode of the reacting system independently. This is called the INM method.[54,59] In this approach, the vibrational energy is just the sum of the vibrational energies within each mode,

$$\epsilon_{vib}(n_1,n_2,\ldots,n_{F-1},s) = \sum_{n=1}^{F-1} \epsilon_{vib,m}(n_m,s) \qquad (18)$$

so that eqs. (15) and (16) are still valid. In order to compute the approximate anharmonic vibrational energy levels of mode m, we must consider the potential energy along this mode, i.e., along the generalized normal coordinate $Q_m(s)$. This coordinate can be expressed as a linear combination of mass-scaled cartesian displacements $\Delta\underset{\sim}{x}$ from the bottom of the vibrational well,

$$Q_m(s) = \Delta\underset{\sim}{x} \cdot \underset{\sim}{L}_m(s) \qquad (19)$$

where $\underset{\sim}{L}_m(s)$ is a column of the unitary matrix $\underset{\approx}{L}(s)$ that diagonalizes the

projected matrix $\underset{\sim}{F}^P(s)$ of eq. (12):[34,59,62]

$$[\underset{\sim}{L}(s)]^T \underset{\sim}{F}^P(s) \underset{\sim}{L}(s) = \underset{\sim}{\Lambda}(s) \tag{20}$$

where a superscript T denotes a transpose. The nonzero eigenvalues $k_{mm}(s)$ of the diagonal matrix $\underset{\sim}{\Lambda}(s)$ are the principal normal-coordinate quadratic force constants, which are related to the normal-mode frequencies (in cm^{-1}) by

$$\bar{\nu}_m(s) = [k_{mm}(s)/\mu]^{\frac{1}{2}}/2\pi c \tag{21}$$

where μ is defined in Sect. 2.1. The potential energy along mode m can be expressed as

$$V_m[Q_m(s),s] = \tfrac{1}{2}k_{mm}(s)[Q_m(s)]^2 + k_{mmm}(s)[Q_m(s)]^3 + \\ + k_{mmmm}(s)[Q_m(s)]^4 + \ldots \tag{22}$$

where $k_{mmm}(s)$, $k_{mmmm}(s)$, etc. are higher-order principal normal-coordinate force constants, and are related to the third, fourth, etc. directional derivatives of the potential energy along the normal-mode direction $\underset{\sim}{L}_m(s)$. While formally correct, eq. (22) is not directly useful for the present discussion because even if sufficient information about the potential energy in the region of the bottom of the well is available for the calculation of the higher-order force constants in eq. (22), for a general polyatomic system with a relatively large number of vibrational modes there is no practical way to use these force constants to obtain accurately the large number of energy levels required by eq. (16). For this purpose, in modes possessing cubic anharmonicity [i.e., $k_{mmm}(s) \neq 0$] it is useful to replace the general potential of eq. (22) by a Morse function,

$$V_{M,m}[Q_m(s),s] = D_e(s)\{\exp[-\beta_{M,m}(s)Q_m(s)] - 1\}^2 \tag{23}$$

where the dissociation energy $D_e(s) = D - V_{MEP}(s)$ and where the range parameter $\beta_{M,m}(s)$ is chosen so that the Morse potential has the correct quadratic force constant at its minimum:

$$\beta_{M,m}(s) = [k_{mm}(s)/2D_e(s)]^{\frac{1}{2}} . \tag{24}$$

We refer to this method of choosing $D_e(s)$ and $\beta_{M,m}(s)$ as the Morse I approximation.[42,51,59] The energy levels of this potential are given by

$$\epsilon_{vib,m}(n_m,s) = hc\bar{\nu}_m(s)(n_m + \tfrac{1}{2})[1 - x_{M,m}(s)(n_m + \tfrac{1}{2})] \tag{25}$$

where $\bar{\nu}_m(s)$ is the harmonic frequency of eq. (21) and $x_{M,m}(s)$ is the

unitless Morse anharmonicity constant given by

$$x_{M,m}(s) = hc\bar{\nu}_m(s)/4D_e(s) \ . \qquad (26)$$

This approach has been shown to provide satisfactory treatments for the bound stretching motion in collinear atom-diatom collisions[10,42,44] as well as for the four vibrational modes of the OH + H_2 system[59] that possess cubic anharmonicity. It should also be pointed out that in many cases the results obtained using the Morse I approximation agree well with those obtained by fitting the Morse function to the true quadratic and cubic force constants of the potential. The Morse I approximation appears to be suitable for general application to vibrational modes possessing cubic anharmonicity, and it has the advantage that it does not require derivatives of the potential higher than second.

Some vibrational modes that, due to symmetry, have no cubic anharmonicity [i.e., $k_{mmm}(s)=0$] cannot be described well by the Morse model. Examples of such modes include bends of linear systems, out-of-plane bends of planar systems, and certain stretching motions (such as the asymmetric stretch in the water molecule). In cases where $k_{mmmm}(s)$ is known, either from differentiating the actual PES or from fitting the potential along the mode to some simple functional form, such modes can be treated by a quadratic-quartic model, which has been shown to provide satisfactory results in atom-diatom systems[43,44,57,58] and for the out-of-plane bending motion in the OH + H_2 system.[59] In this approach, the potential of eq. (22) is truncated after the quartic term and the energy levels for the resulting quadratic-quartic potential are approximated accurately by an analytic procedure obtained by a perturbation-variation method discussed elsewhere.[43,57,63]

Although the INM approach allows for the inclusion of anharmonic effects within each individual mode in a practical and relatively accurate manner, it ignores the couplings between the modes, which have been shown to be quite important for obtaining accurate vibrational partition functions in the H_2O and SO_2 molecules[64] and which are probably also important in describing the bound vibrational motions of a reacting system along the reaction path. Mode-mode couplings are considered in the next subsection.

2.3. Mode-Mode Couplings and Vibrational Energy Calculations for an Internal-Coordinate Force Field

The majority of VTST calculations performed to date have been for atom-diatom collisions.[11] For that kind of collision, reasonably accurate calculations of the vibrational energy levels are possible without excessive labor. For example, for a collinear minimum-energy path the vibrations orthogonal to the path consist of one stretch and a twofold degenerate bend. Use of a curvilinear bend coordinate[43,44,57,65] reduces the bend-stretch coupling, and principal anharmonicity can be included accurately in the bend by the harmonic-quartic approximation described above or by the WKB approximation. The stretch can also be treated accurately by the WKB approximation.[15] It is also possible to estimate the effect of bend-rotational coupling,[57] and in particularly

interesting cases one could realistically do even better. For polyatomic systems, the effort to systematically improve the quantal or semiclassical calculation of the multidimensional bound vibrational energy levels rapidly becomes impractical as the number of atoms increases, especially in the context of canonical VTST calculations, for which a knowledge of a large number of energy levels is required at each location of the dividing surface along the reaction path. Furthermore, the quantal or semiclassical calculation of vibrational energy levels requires detailed information about the PES, while for many polyatomic systems the available information may consist only of a set of geometries, energies, gradients, and quadratic force constants (frequencies) along the reaction path. Strategies different from those used for atom-diatom collisions are thus clearly required for treating the bound vibrational motions in polyatomic reacting systems. One possible element of commonality, however, would be to use curvilinear internal coordinates to reduce mode-mode coupling.

One possible way to include mode-mode couplings in normal coordinates is by perturbation theory. The perturbation-theory expressions for the energies of a polyatomic system are usually given in terms of dimensionless normal coordinates, $\{q_m(s),\ m=1,2,\ldots,F-1\}$. These are related to the mass-scaled normal-coordinates $\{Q_m(s),\ m=1,2,\ldots,F-1\}$ of eq. (19) by

$$q_m(s) = 2\pi[c\mu\bar{\nu}_m(s)/h]^{\frac{1}{2}}Q_m(s) \ . \tag{27}$$

In these coordinates the vibrational potential energy can be evaluated in cm^{-1} by

$$[V(q_1,q_2,\ldots,q_{F-1},s) - V_{MEP}(s)]/hc = \tfrac{1}{2}\sum_i \bar{\nu}_i(s)[q_i(s)]^2 + \\ + \sum_{i\le j\le k} \bar{k}_{ijk}(s)q_i(s)q_j(s)q_k(s) + \\ + \sum_{i\le j\le k\le \ell} \bar{k}_{ijk\ell}(s)q_i(s)q_j(s)q_k(s)q_\ell(s) \tag{28}$$

where $\bar{k}_{ijk}(s)$ and $\bar{k}_{ijk\ell}(s)$ are the cubic and quartic dimensionless normal coordinate force constants (in cm^{-1}), respectively, which are related to the appropriate third and fourth derivatives, respectively, of the potential energy with respect to the dimensionless normal coordinates. We also define $\bar{k}_{211} = \bar{k}_{112}$, etc. Although force constants with $i > j$ do not appear in eq. (28), they do appear below in eq. (30). In eq. (28) we have followed the usual practice of truncating the Taylor series expansion of the potential energy at quartic terms. If the cubic and quartic force constants in eq. (28) are known, they can be related to the vibrational energy via perturbation theory. A standard procedure is to treat cubic terms to second order and quartic terms to first order. This yields:[66]

$$\epsilon_{vib}(n_1,n_2,\ldots,n_{F-1},s)/hc = \sum_i \bar{\nu}_i(s)(n_i+\tfrac{1}{2}) + \sum_{i,j} x_{ij}(s)(n_i+\tfrac{1}{2})(n_j+\tfrac{1}{2}) \quad (29)$$

where, omitting the dependencies on s to simplify the expressions,

$$x_{ii} = \tfrac{1}{4}[6\bar{k}_{iiii} - \frac{15\bar{k}_{iii}^2}{\bar{\nu}_i} - \sum_{j\neq i}(\frac{\bar{k}_{iij}^2}{\bar{\nu}_j})\frac{8\bar{\nu}_i^2 - 3\bar{\nu}_j^2}{4\bar{\nu}_i^2 - \bar{\nu}_j^2}] \quad (30)$$

and

$$x_{ij} = \tfrac{1}{2}\{\bar{k}_{iijj} - \frac{6\bar{k}_{iii}\bar{k}_{ijj}}{\bar{\nu}_i} - \frac{4\bar{k}_{iij}^2\bar{\nu}_i}{4\bar{\nu}_i^2 - \bar{\nu}_j^2} - \sum_{k\neq i,j}\frac{\bar{k}_{iik}\bar{k}_{kjj}}{\bar{\nu}_k} - \tfrac{1}{2}\sum_{k\neq i,j}\bar{k}_{ijk}^2\bar{\nu}_k[\frac{\bar{\nu}_k^2 - \bar{\nu}_i^2 - \bar{\nu}_j^2}{(\bar{\nu}_i+\bar{\nu}_j+\bar{\nu}_k)(\bar{\nu}_i+\bar{\nu}_j-\bar{\nu}_k)(\bar{\nu}_i-\bar{\nu}_j+\bar{\nu}_k)(\bar{\nu}_i-\bar{\nu}_j-\bar{\nu}_k)}]\}. \quad (31)$$

Equations (29)-(31) are for the case of nondegenerate vibrations; the modifications in these equations for degenerate vibrations may be found elsewhere.[66-68] For the discussion below we emphasize that eqs. (29)-(31) are based on a knowledge of the cubic and some of the quartic dimensionless normal coordinate force constants.

As discussed above, the neglect of the normal coordinate interaction force constants often causes a great loss of accuracy. However, for a moderate-sized polyatomic reacting system, the direct calculation of the large number of normal-coordinate interaction force constants at each location of the dividing surface along the reaction path is not only impractical, but also requires more information about the potential energy surface than is usually available. It may be useful in such cases to consider the representation of the potential energy surface in terms of more physically meaningful curvilinear internal coordinates s_a (e.g., bond stretches and bond-angle bends). If we use 3N-6 internal coordinates for an N-atom reactant molecule we may write its potential as:

$$V^R = \sum_{a\leq b} K_{ab}s_a s_b + \sum_{a\leq b\leq c} K_{abc}s_a s_b s_c + \sum_{a\leq b\leq c\leq d} K_{abcd}s_a s_b s_c s_d . \quad (32)$$

In the present treatment we will pay special attention to the case where the s_a are "valence coordinates", which consist of bond stretches, bond-angle bends, out-of-plane bends, and bond torsions.[69] (In the more general case one could also include interpair distances for nonbonded atoms.) If the cubic and quartic interaction force constants are

neglected in such a representation, far less loss of accuracy occurs than when they are neglected in the normal-coordinate representation. This has been explicitly demonstrated in a recent study of the vibrational partition functions for the H_2O and SO_2 molecules.[64] As an example of the differences between the normal coordinate and curvilinear internal coordinate representations of the potential energy embodied in eqs. (28) and (32), respectively, consider the bending and stretching motions in the CO_2 molecule. For geometries near linear, Pariseau et al.[67] showed that, up to the energy corresponding to about ten bending vibrational quanta, the minimum in the potential energy along a C-O bond stretching coordinate, as the bending angle is varied, describes a nearly circular path with a radius equal to the C-O equilibrium bond distance. Thus, in the internal-coordinate representation of the potential energy, the effects of bending and stretching motions are nearly separable (i.e., the interaction internal-coordinate force constants involving the bending and stretching internal coordinates are quite small), while in normal coordinates, which are linear combinations of mass-scaled or mass-weighted cartesians, a circular bending path can result only by substantial bend-stretch couplings of the uncoupled straight-line motions of the nuclei.

A further advantage of representing the potential energy in the internal coordinates is that if the principal anharmonic internal coordinate force constants K_{aaa} and K_{aaaa} cannot be calculated directly from the available information, they can often be predicted sufficiently accurately by modelling the potential energy along a particular curvilinear internal coordinate direction by a simple functional form.[64] For example, bond stretches can be modelled in terms of the quadratic force constant K_{aa} and the dissociation energy D_e by the Morse I approximation described above, and linear A-B-C bending motions can be modelled in terms of the AC diatomic Morse parameters D_e^{AC}, β_M^{AC}, and r_e^{AC} by the anti-Morse bend approximation:[70]

$$V_{AM}(\Phi) = V_{AM}^{AC}[r_{AC}(\Phi)] - V_{AM}^{AC}[r_{AC}(\Phi=\pi)] \ , \tag{33}$$

where Φ is the bond angle,

$$V_{AM}^{AC}(r_{AC}) = (\gamma D_e^{AC}/2)\{2 \exp[-\beta_M^{AC}(r_{AC} - r_e^{AC}) + \\ + \exp[-2\beta_M^{AC}(r_{AC} - r_e^{AC})]\} \ , \tag{34}$$

γ is adjusted to reproduce $K_{\Phi\Phi}$, and $K_{\Phi\Phi\Phi\Phi}$ is obtained by differentiation. Sometimes even quadratic force constants can be estimated;[57,58,70,71] for example, for Cl-H-H generalized transition states, satisfactory results have been obtained with a value of 0.5 for γ.

Neglecting all of the higher-order (cubic and quartic) cross terms in eq. (32) yields the harmonic-general-plus-anharmonic valence force

field (HG/AVFF):[†]

$$V^R = \sum_{a \le b} K_{ab} s_a s_b + \sum_a (K_{aaa} s_a^3 + K_{aaaa} s_a^4) \quad . \tag{35}$$

By repeated application of the chain rule for derivatives, this potential energy can be transformed through quartic terms to the representation in dimensionless normal coordinates of eq. (28) in the standard way.[66,67,72-74] Since the internal coordinates are curvilinear while the normal coordinates are not, this transformation is necessarily nonlinear.

In general the potential may be written as a function of 3N-6 internal coordinates. In some cases, e.g., CH_4, there are more than 3N-6 valence coordinates.[74] One may always delete sufficient coordinates from the list to obtain an independent set.[75] In some cases, however, either to take advantage of symmetry or obtain or use transferable and physically meaningful force constants, it is convenient to use more than 3N-6 internal coordinates. In such a case one or more coordinates are redundant. Another possibility is that a redundancy condition is satisfied only for a restricted range of geometries, including the reference geometry of the force field; this is sometimes called a constraint.[76,77] If redundant coordinates are retained or there is a constraint, linear force constants need not be zero [i.e., terms of the form $K_a s_a$ may appear in eq. (35)].[75,76] Both linear and higher-order force constants become nonunique when redundant coordinates are used.[62a,75]

To use the HG/AVFF as described above, we must first determine the quadratic force field from the available information about the PES. Then the anharmonic terms can be modelled or calculated directly in internal coordinates. If the internal coordinates are independent there is a unique transformation from the normal-coordinate force field to the internal-coordinate one, and in particular a harmonic general force field may be calculated from the normal-coordinate one; alternatively the harmonic general force field may be calculated uniquely from any global PES by the chain rule. If there are redundancies, then these procedures do not yield unique force constants. In such cases one should model the force field directly in internal coordinates or introduce subsidiary conditions on the force constants.

In order to apply the HG/AVFF model to polyatomic generalized transition states, we must reference the bond stretches and bend coordinates to an arbitrary point on the MEP, making them functions of s. We then obtain

---

[†]A valence force field includes only valence coordinates and principal force constants; a general force field also includes interactions. Thus the harmonic valence terms are the principal ones in the first sum in eq. (35), the harmonic general field consists of the whole first sum, and the anharmonic valence terms comprise the second sum.

$$V = \sum_a K_a(s)s_a(s) + \sum_{a\leq b} K_{ab}(s)s_a(s)s_b(s) +$$

$$+ \sum_a \{K_{aaa}(s)[s_a(s)]^3 + K_{aaaa}(s)[s_a(s)]^4\} \qquad (36)$$

where we have included the linear force constants $K_a(s)$ because the first derivatives do not vanish at a general location on the MEP, even for independent, unconstrained internal coordinates. The extension of eq. (36) to include internal-coordinate anharmonic mode-mode couplings is straightforward and simply consists of adding terms like $K_{abc}(s)s_a(s)s_b(s)s_c(s)$ to eq. (36).

The transformation from the internal coordinate force constants $K_a(s)$, $K_{ab}(s)$, etc. to the dimensionless normal coordinate force constants $\bar{k}_i(s)$, $\bar{k}_{ij}(s)$, etc. can be accomplished through a set of several steps. For this purpose it is convenient to employ a dual notation for the atomic cartesian coordinates. Let $i = A_i\gamma_i$ be an index such that A_i can denote any of the atoms A,B,C,..., and γ_i can be x, y, or z. Then the unscaled atomic cartesian coordinates are denoted X_i such that X_1, X_2, and X_3 denote the x, y, and z coordinates of the first atom, X_4, X_5, and X_6 denote the x, y, and z coordinates of the second atom, etc. We then define difference cartesians X_{ij} for $i\neq j$ and $\gamma_i=\gamma_j$ as

$$X_{ij} = X_{A_i\gamma_i A_j\gamma_j} = X_i - X_j \ . \qquad (37)$$

These quantities are not needed for i=j or $\gamma_i\neq\gamma_j$.

For the first step of the transformation, we express the internal coordinates in terms of the difference cartesians. The length of the A-B bond is thus given by

$$r_{AB} = \Big(\sum_{\gamma=x,y,z} X^2_{A\gamma B\gamma}\Big)^{\frac{1}{2}} \qquad (38)$$

while the angle A-B-C can be expressed as

$$\Phi_{ABC} = \cos^{-1}\Big[\Big(\sum_{\gamma=x,y,z} X_{B\gamma C\gamma}X_{B\gamma A\gamma}\Big)/r_{BA}r_{BC}\Big] \ . \qquad (39)$$

Corresponding expressions for the other two types of internal coordinates (out-of-plane bending and torsional angles) are given elsewhere.[78] The difference cartesian force constants k''_{ij}, $k''_{ijk\ell}$, $k''_{ijk\ell mn}$,..., are the derivatives of V with respect to the difference cartesians X_{ij}; X_{ij} and $X_{k\ell}$; X_{ij}, $X_{k\ell}$, and X_{mn};.... These are related to the internal coordinate force constants by the nonlinear transformations:[79]

$$k''_{ij} = \sum_a b^a_{ij}K_a \qquad (40)$$

$$k''_{ijk\ell} = \sum_a b^a_{ijk\ell}K_a + \sum_{a\leq b} b^a_{ij}b^b_{k\ell}K_{ab} \qquad (41)$$

$$k''_{ijk\ell mn} = \sum_a b^a_{ijk\ell mn} K_a + \sum_{a\le b} (b^a_{k\ell mn} b^b_{ij} + b^a_{ijmn} b^b_{k\ell} + b^a_{ijk\ell} b^b_{mn}) K_{ab} + \\ + \sum_{a\le b\le c} b^a_{ij} b^b_{k\ell} b^c_{mn} K_{abc} \qquad (42)$$

and

$$k''_{ijk\ell mnop} = \sum_a b^a_{ijk\ell mnop} K_a + \sum_{a\le b} (b^a_{ijk\ell} b^b_{mnop} + b^a_{ijmn} b^b_{k\ell op} + \\ + b^a_{ijop} b^b_{k\ell mn} + b^a_{k\ell mnop} b^b_{ij} + b^a_{ijmnop} b^b_{k\ell} + b^a_{ijk\ell op} b^b_{mn} + \\ + b^a_{ijk\ell mn} b^b_{op}) K_{ab} + \sum_{a\le b\le c} (b^a_{ijk\ell} b^b_{mn} b^c_{op} + \\ + b^a_{ijmn} b^b_{k\ell} b^c_{op} + b^a_{ijop} b^b_{k\ell} b^c_{mn} + b^a_{k\ell mn} b^b_{ij} b^c_{op} + \\ + b^a_{k\ell op} b^b_{ij} b^c_{mn} + b^a_{mnop} b^b_{ij} b^c_{k\ell}) K_{abc} + \\ + \sum_{a\le b\le c\le d} b^a_{ij} b^b_{k\ell} b^c_{mn} b^d_{op} K_{abcd} \qquad (43)$$

where we have omitted the argument s on all coefficients, and the new coefficients, b^a_{ij}, $b^a_{ijk\ell}$, etc. are the partial derivatives of internal coordinate a with respect to difference cartesian X_{ij}, difference cartesians X_{ij} and $X_{k\ell}$, etc. These coefficients may be expressed analytically for each type of internal coordinate.[67,74,78] Some examples are given in the Appendix.

In the second step of the transformation, the difference cartesian force constants $k''_{ij}(s)$, $k''_{ijk\ell}(s)$, etc. are converted to mass-scaled cartesian force constants $k'_i(s)$, $k'_{ij}(s)$, etc. From the definition of the difference cartesians given in eq. (37), it is easily seen that this transformation is linear and that the transformation coefficients are given by (with x_i a mass-scaled cartesian):

$$t^i_{op} = \frac{\partial X_{op}}{\partial x_i} = \left(\frac{\mu}{m_{A_o}}\right)^{\frac{1}{2}} \delta_{oi} - \left(\frac{\mu}{m_{A_p}}\right)^{\frac{1}{2}} \delta_{pi} \qquad (44)$$

where m_{A_p} is the mass of atom A_p and μ is defined in Sect. 2. This transformation may then be written explicity as

$$k'_i(s) = \sum_{m<n} k''_{mn}(s) t^i_{mn} \qquad (45)$$

$$k'_{ij}(s) = \sum_{m<n\le o<p} k''_{mnop}(s) t^i_{mn} t^j_{op} \qquad (46)$$

$$k'_{ijk}(s) = \sum_{m<n\leq o<p\leq q<r} k''_{mnopqr}(s) t^{i}_{mn} t^{j}_{op} t^{k}_{qr} \tag{47}$$

and

$$k'_{ijk\ell}(s) = \sum_{m<n\leq o<p\leq q<r\leq s<t} k''_{mnopqrst}(s) t^{i}_{mn} t^{j}_{op} t^{k}_{qr} t^{\ell}_{st} \ . \tag{48}$$

The array $k'_i(s)$ is just grad V in mass-scaled cartesians. In the third step of the force constant transformation, we project out of $k'_{ij}(s)$ the contributions from motion along the reaction path and from overall rotations and translations,[34,59] as discussed above, and diagonalize the projected matrix. The nonzero eigenvalues $k_{mm}(s)$ provide the generalized normal-mode frequencies $\bar{\nu}_m(s)$ via eq. (21), and the associated eigenvectors $L_m(s)$ [the columns of the matrix $\tilde{L}(s)$ of eq. (20)] yield the generalized normal modes. The dimensionless normal coordinates are then given by

$$q_m(s) = \Delta \underset{\sim}{x} \cdot \underset{\sim}{\ell}_m(s) \tag{49}$$

where

$$\underset{\sim}{\ell}_m(s) = 2\pi[c\mu\bar{\nu}_m(s)/h]^{\frac{1}{2}} \underset{\sim}{L}_m(s) \ . \tag{50}$$

The fourth and final step of the transformation of the force constants from difference cartesians to dimensionless normal coordinates, i.e., the transformation from mass-scaled cartesian coordinates to dimensionless normal coordinates, is thus linear and is given for the cubic and quartic force constants appearing in eqs. (30) and (31) by

$$\bar{k}_{ijk}(s) = \sum_{m\leq n\leq r} k'_{mnr}(s) \ell_{im}(s) \ell_{jn}(s) \ell_{kr}(s) \tag{51}$$

and

$$\bar{k}_{ijk\ell}(s) = \sum_{m\leq n\leq r\leq u} k'_{mnru}(s) \ell_{im}(s) \ell_{jn}(s) \ell_{kn}(s) \ell_{\ell u}(s) \ . \tag{52}$$

Having obtained the dimensionless normal coordinate force constants from those in internal coordinates, eqs. (29)-(31) can be used to obtain the perturbation theory approximation to the vibrational energy levels.

In many cases the energy levels predicted by perturbation theory will be sufficiently accurate and the above scheme will be completely satisfactory. This will be true especially for calculating $V_a^G(s)$ or $\Delta G_T^{GT,O}(s)$ at low T. However for moderately large anharmonicity or higher-energy levels, the accuracy of perturbation theory becomes worse.[64,68,80] An alternative procedure for estimating the vibrational partition function in such cases is the Pitzer-Gwinn method.[64,81,82] This method is based on the fact that the ratio $\tilde{Q}_{vib}(T,s)/\tilde{Q}^H_{vib}(T,s)$ of the anharmonic to harmonic quantal partition functions, with the zero of energy located at the zero-point level (indicated by the tilde), is given correctly by the corresponding ratio $Q_{vib,C}(T,s)/Q^H_{vib,C}(T,s)$ of classical (C) partition functions in both the low- and high-temperature limits. The approximation is to assume that this relationship holds at

all temperatures. The quantal anharmonic partition function $\tilde{Q}_{vib}(T,s)$ is thus approximated as

$$\tilde{Q}_{vib}(T,s) \cong \tilde{Q}^{H}_{vib}(T,s)[Q_{vib,C}(T,s)/Q^{H}_{vib,C}(T,s)] \ . \qquad (53)$$

This approach has already been shown to provide accurate results for the vibrational partition functions of the bound molecules H_2O and SO_2,[64] and eq. (53) should be equally applicable for generalized transition states. The harmonic partition functions are given by[81]

$$Q^{H}_{vib,C}(T,s) = \prod_{i=1}^{F-1} \tilde{k}T/[hc\bar{\nu}_i(s)] \qquad (54)$$

and

$$\tilde{Q}^{H}_{vib}(T,s) = \prod_{i=1}^{F-1} \{1 - \exp[-hc\bar{\nu}_i(s)\beta]\}^{-1} \ . \qquad (55)$$

The classical anharmonic partition function for the potential of eq. (28) is[83]

$$Q_{vib,C}(T,s) = (2\pi\mu\tilde{k}T/h^2)^{(F-1)/2} \int dQ_1(s)\ldots dQ_{F-1}(s) \times \exp\{-\beta[V - V_{MEP}(s)]\} \qquad (56)$$

where the integrations are over the range $(-\infty,+\infty)$ in mass-scaled normal coordinates defined by

$$Q_m(s) = [h/c\mu\bar{\nu}_m(s)]^{\frac{1}{2}} q_m(s)/2\pi \ . \qquad (57)$$

Contributions from energies greater than $D-V_{MEP}(s)$ should be excluded from the integrand. For small systems the integration can be performed conveniently by Gauss-Hermite quadrature formulas, while for larger systems Monte Carlo numerical integration[84-86] may be more efficient. The anharmonic partition function $Q_{vib}(T,s)$, with the zero of energy located at the bottom of the well, can then be obtained by combining $\tilde{Q}_{vib}(T,s)$ with the zero point energy calculated from eq. (29) by:

$$Q_{vib}(T,s) = \tilde{Q}_{vib}(T,s)\exp[-\beta\varepsilon_{vib}(0,0,\ldots,0,s)] \ . \qquad (58)$$

A possible pitfall in the approach discussed above is that the effective potential energy surface of eq. (28) may not provide an accurate representation of the true potential energy surface in a large enough region about the bottom of the vibrational well, i.e., in the region about the bottom of the well where the integrand of eq. (56) is significant. For example, large cubic or large negative quartic force constants can lead to large, anomalous wells in the effective potential energy that cause great difficulty in the convergence of the numerical integration for $Q_{vib,C}(T,s)$. In such cases, one may need to resort to different choices for the models assumed for the potential energy along the internal-coordinate directions, or to calculating explicitly the third and fourth

derivatives of the potential energy with respect to the internal coordinates, or to global fitting techniques such as discussed in Sect. 4. In such cases it may be advantageous to use eq. (56) but with V in internal coordinates. Thus, rather than transform the internal-coordinate expression for V to normal coordinates through quartic terms before evaluating eq. (56), one may numerically calculate the internal coordinates and the untransformed V for each point in the quadrature grid as eq. (56) is evaluated. This has the advantage that globally meaningful untruncated potential approximations (like the Morse I approximation[42,51]) may be employed in internal coordinates to ensure a well behaved potential for eq. (56), and the truncated normal-coordinate expression need be used only to estimate the zero point energy.

Since we have emphasized second-order perturbation theory in this section, it might be useful to point out that the effect of the $B_{kk'}(s)$ nonadiabatic coupling elements could also be included by second-order perturbationtheory, using a procedure analogous to that of Barton and Howard.[87]

We have concentrated on vibrations in this section and have not considered hindered rotations, Coriolis coupling, or related complications. These kinds of complications will be at least as important for generalized transition states as for bound molecules, and these complications will have to be addressed in future work.

Another approach to including mode-mode coupling in the hybrid rate constant is to perform a multidimensional, nonseparable quantal Monte Carlo calculation. Voter[88] has recently given a convenient formulation that could be applied to $\Delta G_T^{GT,0}(s)$. It includes quantal effects by a Fourier expansion of Feynmann path integrals[89] and allows for importance sampling as required for Monte Carlo calculations on processes with high activation energy. This formulation would be expected to be particularly convenient if the transmission coefficient is close to unity and hence need not be evaluated. When the transmission coefficient is to be calculated also, one requires $V_a^G(s)$. This can be calculated from the zero-temperature limit of $\Delta G_T^{GT,0}(s)$ or by calculating the zero point energies from a reaction-path Hamiltonian. The use of different methods for $\Delta G_T^{GT,0}(s)$ at $T \neq 0$ and $V_a^G(s)$ may be justified by (i) the sensitivity of low-temperature results to very small energy errors, which are hard to make completely negligible in a Monte Carlo calculation, and (ii) the increasing importance of anharmonicity, and hence nonseparability of the normal modes, as T increases.

3. DETERMINATION OF THE REACTION-PATH HAMILTONIAN FROM AB INITIO CALCULATIONS

One of the most important advances achieved in ab initio electronic structure theory in the last 15 or so years has been the capability of determining analytic gradients of energies computed from many types of wavefunctions.[90-100] The gradient of the energy is the vector of partial derivatives of the energy with respect to each of the cartesian coordinates of the molecule or an equivalent set of internal coordinates.[91] Gradients are extremely valuable in locating and

characterizing stationary points on multidimensional PES's.[101-104] There are two advantages of using analytic gradients rather than multiple evaluations of the energy followed by numerical differentiation. First, the analytic gradients are more reliable because there are no artifacts caused by a poor choice of step size. Second, the use of analytic gradients is computationally much more efficient. Using a crude approximation to numerically determine the gradient for a nonlinear polyatomic molecule with N atoms and 3N-6 degrees of freedom requires 3N-5 energy calculations while only one calculation, which is 2 to 5 times longer than one energy calculation, is required for determining analytic gradients.[91] Thus the use of analytic gradients becomes more efficient computationally as the number of atoms N increases. The use of analytic gradients makes the calculation of stationary points (reactant, product, and saddle point geometries) computationally feasible for a large number of reacting systems with 3 or more atoms.

With the availability of analytic gradients, numerical second derivative matrices have been determined and employed in more efficient algorithms for locating stationary points.[101-106] Also, for many types of wavefunctions analytic second derivatives are computationally feasible to determine.[93,97,98,107-111] One gains the same advantages over numerical differentiation using analytic second derivatives as already discussed for using analytic gradients. Furthermore, analytic second derivatives do not contain artifacts from a non-optimal distribution of points used in the numerical determination of the second-derivative matrix. Finally, it should be noted that even though ab initio analytic second derivatives are not currently coded for all types of correlated wavefunctions, the general formulas for determining analytic second derivatives for most types of wavefunctions have been derived[112,113] and we can look forward to their computer implementation. (Even higher derivatives are realizable with the recent calculation of analytic third derivatives for an SCF H_2O calculation.[114]) In summary, state-of-the-art ab initio techniques can provide analytic gradients for most types of wavefunctions and analytic second-derivative matrices for many types of wavefunctions for systems with several ($2 < N < 10$) atoms.

Given these techniques, the determination of a useful RPH for a chemical reaction can proceed at several levels of approximation. The first step in determining the RPH is locating the stationary points that correspond to the reactant, product, and saddle point geometries of the reaction system. The vibrational frequencies and normal mode directions as well as the imaginary frequency corresponding to the reaction coordinate can be determined by diagonalizing the second derivative matrix for the system, and cubic force fields can be obtained by numerical first derivatives of second derivative matrices. In Subsect. 3.1 we discuss determining the RPH from this first level of information; namely, the potential energy and quadratic or cubic force fields at the reactants, products, and saddle point geometries. At each of these geometries the gradient is zero. To calculate the potential along the reaction path (MEP) requires following the path of steepest descent in mass-scaled or mass-weighted coordinates from the saddle point to both the reactant and product geometries. Computationally, this requires taking an initial step off the saddle point in both the product and

reactant directions along the direction of the normal mode with the imaginary frequency and then following the path of steepest descent along the direction of the negative gradient. At each point along the reaction path, the frequencies of the vibrations that are orthogonal to the reaction path can be determined by eqs. (20) and (21). Thus, using state-of-the-art computer hardware and ab initio methods, the determination of the reaction path and RPH is feasible for many systems of chemical interest. In Subsect. 3.2 we will discuss some significant practical problems to consider when using ab initio methods to determine an RPH.

3.1. Simple Interpolatory Methods for Reaction Path Calculations

Although RPH's based upon ab initio calculations of the reaction path and the vibrational frequencies perpendicular to the reaction path have been determined for several polyatomic systems (see, e.g., Refs. 7, 115-119), there are many polyatomic reactions for which a set of high quality ab initio calculations along the reaction path is currently not computationally feasible. However, for many such systems it is feasible to optimize the geometries and determine the vibrational frequencies at the set of stationary points along the reaction path, including any saddle point geometries. In such cases one possible way of constructing an RPH is by interpolating the geometry, the potential energy, and the vibrational frequencies along the reaction path by using information either pertaining solely to the stationary points or based on a small number of points including the stationary points.[120] This approach has been applied successfully to collinear A + BC reactions.[120] For the high-barrier reactions H + H_2 → H_2 + H and Cl + HD → HCl + D, the potential energy and the real vibrational frequency in the vicinity of the saddle point were fit to quadratic functions in s. For the reactions F + H_2 → HF + H and I + H_2 → HI + H, which have small intrinsic barrier heights, an asymmetric Eckart barrier[121,122] and a gaussian form were used to model the barrier while an exponential form similar to that used by Quack and Troe[123,124] for triatomic dissociation reactions was used to represent the vibrational frequency. Reaction probabilities based upon classical microcanonical variational transition state theory[51] were determined and compared for both the interpolated RPH and the exact RPH of the global potential energy surfaces[125-128] for each of these reactions. The results from this investigation indicate that the interpolation method works reasonably well for estimating the reaction probability, even though it fails to predict the position of the generalized transition state dividing surface with high accuracy. In particular, for the systems studied, the error in the reaction probabilities is at most 18% while the predicted deviation of the variational transition state from the saddle point differs as much as 260% from the predicted position using the noninterpolated RPH. Nonetheless, it is very encouraging that reasonable reaction probabilities could be obtained using this interpolation scheme based upon a minimal amount of information concerning the reaction path. Notice that because three points were used in the vicinity of the saddle point, the method is equivalent to using numerical differentiation of the saddle point quadratic force

field. If anharmonicity is neglected, one can perform conventional transition state theory calculations based on quadratic force fields for reactants and products, but with a generalization of the method of Ref. 120, one can perform approximate VTST calculations if one simply adds the cubic or cubic and quartic force constants at the saddle point.

An even simpler method, but one which will often be much less reliable, is to interpolate based only on quadratic force fields at the stationary points. Recently, Carrington et al.[129] have approximated the RPH for the isomerization of vinylidene to acetylene using an interpolation method based solely on a set of ab initio energies and force constants at four stationary points along the reaction path (vinylidene, acetylene, and two symmetrically equivalent transition states). The potential energy along the reaction path was interpolated by an even sixth-order polynomial, and a quadratic form was used for interpolating the vibrational frequencies of the vibrational modes perpendicular to the reaction path. These authors also included the $\mathcal{B}_{kF}(s)$ curvature components and the $\mathcal{B}_{kk'}(s)$ nonadiabatic coupling coefficients in their RPH, and they fit these to a quadratic form.

Other workers[130] have employed gaussian-type functions for fitting the curvature as a function of the reaction coordinate. In many A + BC reactions, curvature is not a simple function of s and the reaction probabilities are very sensitive to it. Attempts to approximate the curvature in such cases led to large quantitative errors;[131] however, Carrington et al.[129] used their RPH to calculate the lifetime of vinylidene and these lifetime calculations were not as sensitive to reaction-path curvature as are most of the tunneling probabilities that have been studied in our group. Thus Ref. 129 provides an instructive example of obtaining an interpolated RPH from a minimal amount of ab initio data.

In this subsection we have presented two examples of calculations where the RPH required for dynamical calculations has been based upon an interpolation of the potential energy, vibrational frequencies, and curvature and nonadiabatic coupling coefficients from a knowledge of PES properties at a small number of points along the reaction path. We pointed out, however, that if attention is restricted only to stationary points, one will generally obtain an accurate approximation to the dependence of the vibrational frequencies on the reaction coordinate in the vicinity of the saddle point only if the input data includes at least some of the third and fourth, as well as the second, derivatives at the saddle point.[120] Simple interpolatory schemes may be the only feasible method for investigating systems with many atoms and degrees of freedom. Nonetheless, further work comparing and refining these schemes is needed before the results can be considered reliable.

3.2. Steepest-Descent-Path Calculations for Constructing RPH's

In this subsection we discuss several practical considerations that arise when constructing RPH's for polyatomic systems from a set of ab initio calculations of the energy, gradient, and force constant matrix at a series of points along a reaction coordinate. To illustrate some of these considerations, we will use the $CH_3 + H_2 \rightarrow CH_4 + H$ reaction and the inversion "reaction" of NH_3 as examples. For the $CH_3 + H_2$ reaction,

two different kinds of empirical global PES's have been proposed in the literature[132-134] (and are discussed in Sect. 4), and several sets of ab initio calculations have also been carried out.[117,135-147] For the NH_3 inversion, Wolfsberg and coworkers[148] have proposed an empirical PES based in part on an accurate anharmonic force field. We have used Raff's global PES for the $CH_3 + H_2$ reaction and Wolfsberg's for the ammonia inversion to construct RPH's. We used the former RPH for VTST and semiclassical tunneling calculations of the abstraction rate constant, and we used the latter to calculate the splitting of the two lowest-energy vibrational levels caused by tunneling through the low (5.2 kcal/mol) inversion barrier.

First, we consider the problem of following the gradient to determine the MEP and the functions $V_{MEP}(s)$ and $V_a^G(s)$. As mentioned above, this requires following the path of steepest descent by taking steps in the direction of the negative gradient. However, when one uses a finite step size, one "zigzags" back and forth across the true MEP. Thus a compromise must be reached between using a small enough step size that the true MEP is followed very closely, and using a large enough step size that the number of ab initio calculations is affordable.

For ab initio calculations of RPH's in the literature, it has not always been stated what step size was used, but practical considerations have apparently dictated the use of fairly large steps. We will now discuss a few examples where step sizes are given in the literature, in each case expressing the step size in mass-weighted cartesians rather than mass-scaled cartesians because the mass-weighted choice makes it easier to compare different systems. Gray et al.[116] used a step size of $0.19\ u^{\frac{1}{2}}a_0$ for studying the HNC → HCN isomerization, and they did find oscillations of the computed MEP; however, they were able to smooth these oscillations by "hand" since only a small portion of the reaction path was required for determining tunneling probabilities in their application. Similarly, Schmidt et al.[149] stated that they typically used steps of $0.15\ u^{\frac{1}{2}}a_0$ in their study of the rotational barrier in silaethylene. In this study, these authors used the method of Ishida et al.[150] for stabilizing the oscillations in the calculated MEP. In particular, they performed an energy minimization along the bisector of the angle formed by the normalized negative gradients from two adjacent calculated points to return to the true MEP. In another example, for the isomerization $CH_3O \rightarrow CH_2OH$, Colwell and Handy[118,151] used a step size of $0.05\ u^{\frac{1}{2}}a_0$ near the saddle point and followed the gradient with a step of $0.1\ u^{\frac{1}{2}}a_0$ when $V_{MEP}(s)$ was about 40% below the value of the $V_{MEP}(s)$ at s=0.

Experience in our group in studying the dynamics of many A + BC type reactions[10,13,15,16,18-28,42,44,51-53,70,122,131] has indicated that small step sizes are necessary, especially when the oscillations are not stabilized. For production runs on A + BC reactions we have used step sizes in the range 4×10^{-5} to $2 \times 10^{-3}\ u^{\frac{1}{2}}a_0$. To investigate this point further for the present discussion, we have graphically examined the convergence properties of the calculated MEP and $V_{MEP}(s)$ and $V_a^G(s)$ curves with respect to the step size for the reactions $H + H_2$, $OH + H_2$, and $CH_3 + H_2$. In these studies we used the global PES's of Truhlar and Horowitz,[152] Schatz and Elgersma,[60] and Raff,[132]

respectively; the gradients were analytically evaluated; and the force constants were determined by converged numerical differentiation. The harmonic oscillator approximation was used in treating the vibrations that are perpendicular to the reaction path. The MEP's were computed using step sizes ranging from 7×10^{-2} to 1.3×10^{-4} $u^{\frac{1}{2}}a_0$. Figures 1 and 2 illustrate the resulting computed $V_{MEP}(s)$ and $V_a^G(s)$ curves, respectively, for the $CH_3 + H_2$ reaction. These figures show that both $V_{MEP}(s)$ and $V_a^G(s)$ are quite sensitive to the step size, and they are only well converged when the step size is 1×10^{-3} $u^{\frac{1}{2}}a_0$ or less. Severe oscillations occur in the $V_a^G(s)$ curve computed using step sizes greater than 1×10^{-3} $u^{\frac{1}{2}}a_0$, and these would have a large effect on rate constant calculations. Figure 1 also illustrates the cautionary fact that, even though the $V_{MEP}(s)$ curve resulting from a calculation with a large step size may be smooth, it is not necessarily converged. Similar results were obtained for the $H + H_2$ and $OH + H_2$ reactions, for which the MEP's seem reasonably well converged for step sizes of 1×10^{-2} to 1×10^{-3} $u^{\frac{1}{2}}a_0$, respectively. In previous work on the $OH + H_2$ system where more stringent convergence criteria were employed, a step size of 1.3×10^{-4} $u^{\frac{1}{2}}a_0$ was used.[59] Furthermore, it was demonstrated for this system that, when using very small step sizes, the stabilization method of Ishida *et al.*[150] actually slowed convergence of the calculated MEP.[59] These results are all consistent in indicating that relatively small step sizes are required for obtaining converged MEP and $V_{MEP}(s)$ and $V_a^G(s)$ curves for reactive systems.

A second point to consider in constructing $V_a^G(s)$ is that if numerical differentiation is used to calculate the force constant matrix, then the results may be sensitive to the distribution of points and the step size used in the difference formulas. We have found that frequencies calculated using the GAMESS[153] codes can vary significantly based upon using 2- or 3-point numerical differentiation formulas and a step size ranging from 0.01 to 0.0001 a_0. Of course, for SCF calculations this problem is eliminated with the use of analytic second derivatives as used by Colwell and Handy.[118,151]

Another kind of difficulty emerges in calculating the MEP and $V_{MEP}(s)$ and $V_a^G(s)$ curves for an isomerization reaction. For such reactions, $V_{MEP}(s)$ and $V_a^G(s)$ have double-well character. We will use the inversion of NH_3 as an example. In this case, because of symmetry, we need to compute the RPH only for one side of the saddle point. We will use the left side for our example. To determine the MEP in the barrier region between the well and the saddle point, one follows the negative gradient from the D_{3h} saddle point structure towards the C_{3v} equilibrium structure. In this case since one is proceeding to the left, s is decremented at each step, starting at zero. To determine the MEP on the other side of the minimum, one starts from points high on the repulsive wall beyond the well and follows the negative gradient in toward the well. While carrying out this step we don't know an absolute origin for s that is consistent with the scale to the right of the minimum so we use a temporary origin at the initial point. The reaction coordinate referred to this temporary origin is called $\hat{s}$. Since we are proceeding to the right, $\hat{s}$ is incremented at every step. One places the initial points higher and higher on the potential until $V_{MEP}(\hat{s})$ and $V_a^G(\hat{s})$ in the

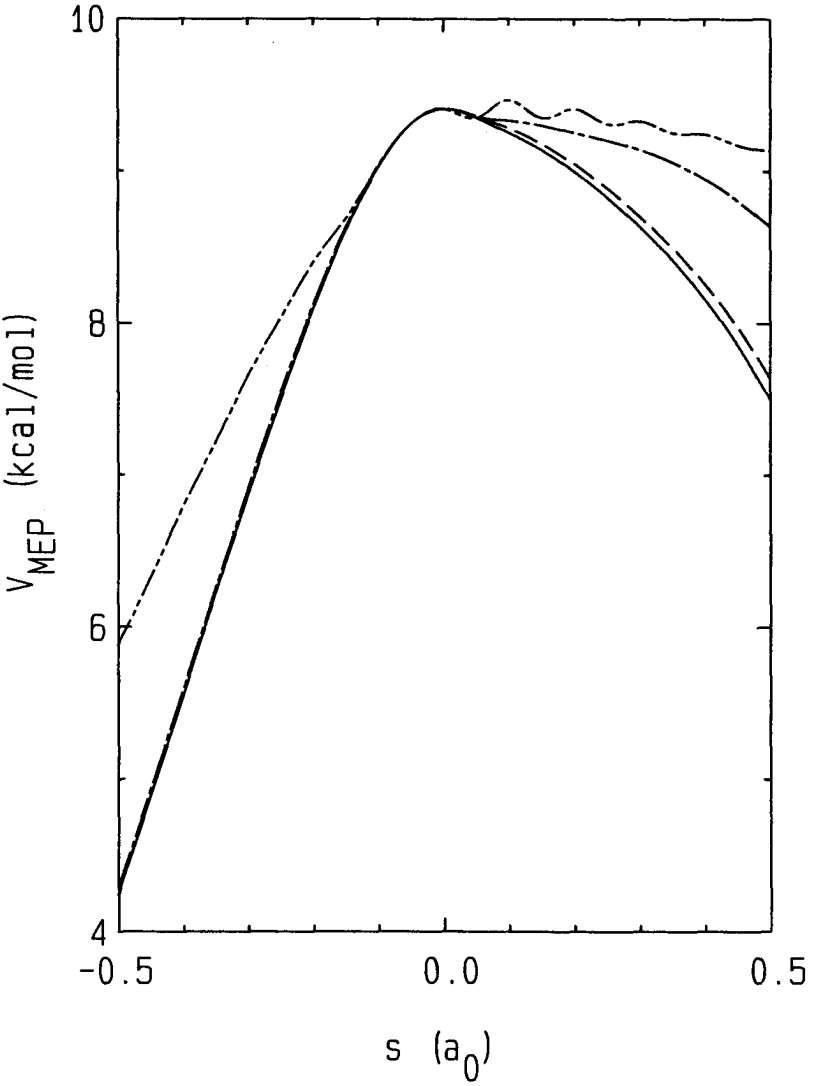

Fig. 1. The potential energy as a function of the distance along the calculated MEP (through mass-scaled coordinates with $\mu = m_{CH_3}m_{H_2}/m_{CH_5}$) for the $CH_3 + HH' \rightarrow CH_4 + H'$ reaction on the Raff potential energy surface. The zero of V_{MEP} is taken to be at the $CH_3 + HH'$ asymptote. The different curves correspond to using different step sizes in following the path of steepest descent to determine the MEP. The step sizes of the curves are: 0.050 a_0 (— — —), 0.025 a_0 (— — -), 0.010 a_0 (— — —), and 0.001 a_0 (——). Results for 0.0001 a_0 would be superimposable on those for 0.001 a_0 to within plotting accuracy. To convert these step sizes to mass-weighted coordinate space, multiply by $\mu^{\frac{1}{2}}$.

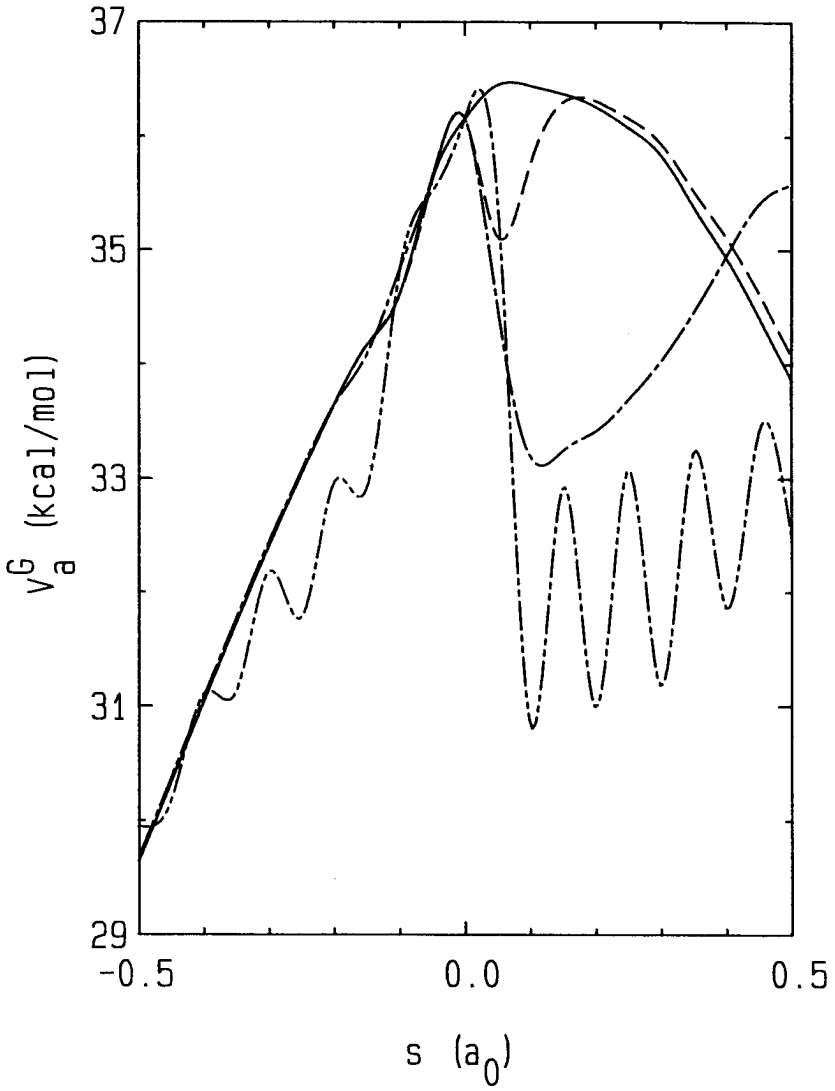

Fig. 2. The ground-state adiabatic potential energy as a function of the distance along the calculated MEP for the CH_3 + HH' → CH_4 + H' reaction on the Raff potential energy surface. The zero of energy is CH_3 + HH' at classical equilibrium; thus the curve tends to the zero point energy of the reactants at $s = -\infty$. The different curves correspond to using different step sizes in following the gradient to determine the MEP. The key for the curves is the same as in Fig. 1, and again the results for 0.001 a_0 and 0.0001 a_0 are superimposable within plotting accuracy.

low-energy region of dynamical interest have converged with respect to the location of the starting point.

To perform the tunneling calculations we require a smooth $V_a^G(s)$ curve for this double-well system. From following the negative gradient starting at the saddle point we determined $V_{MEP}(s)$ and $V_a^G(s)$ for the region to the right of the equilibrium NH_3 structure. Similarly, by following the negative gradient starting from high on the potential and proceeding to the well, we determined $V_{MEP}(\hat{s})$ and $V_a^G(\hat{s})$ to the left of the equilibrium structure. However, a special problem arises in following the negative gradient as one approaches the minimum from either direction, since the gradient approaches zero, and the reaction path calculated with practical-sized steps may show significant zigzagging. This causes the distance along such a path to be artificially longer than the distance along the true MEP and also introduces other errors. Thus we must handle three problems: (i) correct for the elongation of $V_a^G(\hat{s})$ and $V_a^G(s)$ near the minimum, (ii) convert $\hat{s}$ values to s values, and (iii) smoothly join $V_a^G(\hat{s})$ and $V_a^G(s)$ at the minimum to form a continuous $V_a^G(s)$ curve.

To correct for the elongation of the MEP and the resultant errors in $V_a^G(\hat{s})$ and $V_a^G(s)$ we assume that the elongation only occurs when $V_{MEP}(\hat{s})$ or $V_{MEP}(s)$ is less than 0.1 kcal/mol above $V_{MEP}(s)$ at the equilibrium structure, which is taken to be the zero of energy. Therefore we fit $V_{MEP}(\hat{s})$ and $V_{MEP}(s)$ from regions where they lie between 0.1 and 0.2 kcal/mol to the following forms:

$$V_{MEP}(\hat{s}) = \hat{a}(\hat{s} - \hat{s}_0)^2 + \hat{b}(\hat{s} - \hat{s}_0)^3 \tag{59a}$$

and

$$V_{MEP}(s) = a(s - s_0)^2 + b(s - s_0)^3 \ . \tag{59b}$$

In these equations a, $\hat{a}$, b, $\hat{b}$, s_0, and $\hat{s}_0$ are the fitting parameters, of which only the last two will be used. The value obtained for s_0 represents the location along the reaction coordinate of the equilibrium structure of NH_3. Then $\hat{s}$ is converted to s by the following change of origin:

$$s = \hat{s} - \hat{s}_0 + s_0 \ . \tag{60}$$

At this point we have two segments of $V_a^G(s)$ available, one for $s < s_0$ and one for $s > s_0$. We also know $V_a^G(s_0)$ accurately from a standard vibrational analysis at the equilibrium geometry; this was performed prior to any MEP calculations. By connecting the $V_a^G(s)$ functions smoothly together at s_0, consistent with $V_a^G(s_0)$, we will have corrected for the effects of numerical zigzagging. This is accomplished by simultaneously fitting the data from both sides of s_0, using only data where the values of these curves are between 0.1 and 0.2 kcal/mol above $V_a^G(s_0)$. These data are then fit to the following functional form:

$$V_a^G(s) = V_a^G(s_0) + A(s - s_0) + B(s - s_0)^2 + C(s - s_0)^3 \quad . \qquad (61)$$

The final $V_a^G(s)$ curve is a spline fit to a set of values on a grid. When $V_a^G(s)$ at the grid point is greater than $V_a^G(s_0) + 0.2$ kcal/mol, the directly computed value is used as input to the spline routine; but when $V_a^G(s)$ is less than this the input to the spline routine is calculated from eq. (61). The final vibrational energy level splitting was the same when this procedure was repeated with the cubic term missing in eq. (61) so we assume that the order of the polynomial in eq. (61) is sufficiently high to represent the $V_a^G(s)$ curve within 0.2 kcal/mol of its minimum.

With the continuing development of computer hardware and ab initio methods and codes, the construction of RPH's for polyatomic systems may become routine. However, at present, care must be exercised in using ab initio results to achieve a practical balance between affordability and distortions in the results because of errors in following the gradient with an unconverged step size. One avenue that might provide fertile ground for exploration would be to use interpolation methods like those discussed in Subsect. 3.1 in conjunction with input data at increasing numbers of ab initio points along the reaction coordinate. This might provide a reliable and cost effective method for constructing RPH's based upon ab initio data.

4. GLOBAL POTENTIALS

Although, as discussed in Sect. 2, there are still significant difficulties in the practical treatment of anharmonicity and mode coupling, VTST and semiclassical tunneling calculations have reached a high enough state of development that in practical applications the accuracy of a calculated thermal rate constant will usually be more limited by the uncertainties in the potential energy surface than by the errors introduced by the approximate treatment of the dynamics. The ab initio steepest-descent-path techniques discussed in Sect. 3 provide one promising avenue for supplying the required PES data. In many cases though one will require a more global PES, either because large-curvature tunneling paths must be considered or because semiempirical adjustments are to be considered or both. In attempting either to construct semiempirical surfaces or to fit ab initio calculations, we require flexible analytic procedures. The difficulty of reliably representing PES data in an analytic form when it is available or obtainable has been just as serious of a stumbling block in recent years as has been the uncertainty in, and the difficulty of generating, the original data. In this section we will address some of the issues involved in the analytic representation of PES's or RSP's for polyatomic systems.

A promising starting point in the design of polyatomic PES's is to extend in some manner the methods that have been used with success for atom-diatom PES's. This should be an especially promising approach when one only requires an accurate potential in the reaction swath for an atom-transfer reaction where at most two bond lengths differ

significantly from their equilibrium values. One example of this approach was developed by Raff[132] and applied to $CH_3 + HT \leftrightarrow CH_4 + T$. This method, which is a polyatomic generalization of the multiparameter LEPS scheme (MLEPS)[154,155] that has been applied so successfully to A + BC reactions, seems to us to have a number of practical advantages. One advantage of this procedure is that the MLEPS scheme can be made very flexible by making the Sato parameters explicit functions of local variables such as internal angles or bond lengths.[156,157] For A + BC this allows one to make localized changes in the PES, and the hope is that one can embed this same flexibility in a polyatomic surface by starting with the MLEPS function for the dependence of the potential on the lengths of bonds that are made and broken. A worthwhile goal for this kind of treatment is to obtain a functional form for which one can refine one area of the surface in order to agree with ab initio calculations or experimental data without changing the rest of the surface.

In Raff's PES for $CH_3 + HT$, the potential is a sum of four three-center MLEPS potentials, one for each of the C-H-T moieties, and an angle-dependent term to control the change of the methyl moiety from trigonal planar to tetrahedral. By breaking up the potential in this manner, Raff reduced the problem of modelling a six-body interaction to that of modelling several three-body ones.

Table I compares the saddle point characteristics of the Raff surface to those calculated by the ab initio polarization-configuration-interaction (PolCI) method.[144,145] The Raff surface has a lower and earlier, but also thinner barrier. Since, all other things being equal, one expects higher barriers to have higher imaginary frequencies, it

TABLE I

Saddle point characteristics

Quantity	PolCI[a]	Raff[b]
R_{C-H_1,H_2,H_3} (a_0)	2.04	2.07
R_{C-H_4} (a_0)	2.78	3.02
$R_{H_4-H_5}$ (a_0)	1.74	1.48
$V^{\ddagger}$ (kcal/mol)[c]	10.7	9.4
$\bar{\nu}^{\ddagger}$ (cm^{-1})	974i	1478i

[a] Ref. 144 and 145

[b] Ref. 132

[c] relative to $CH_3 + H_2$.

poses an interesting challenge to try to adjust the Raff surface to agree better with the ab initio one for all these characteristics.

The basic design of the Raff surface suggests that the methods for localized adjustments mentioned above for atom-diatom MLEPS potentials could be used to correct the discrepancies between the Raff surface and the PolCI calculations. In these methods single parameters in the MLEPS function are replaced by functional forms. The functional forms used should be chosen such that except for a localized region of strong interaction, they go smoothly to the values required to give the surface its correct asymptotic limits and general global form. The "turning off and on" of these localized functional forms is best accomplished through the use of switching functions. When choosing an appropriate switching function it is important to maintain the analyticity of the PES at least through second derivatives and preferably through fourth derivatives. Flexibility can be built in by using adjustable parameters in exponential, hyperbolic, and gaussian functions.

A problem that sometimes occurs in reaction-path Hamiltonians, especially for bend potentials,[118,151,158] is the bifurcation of the reaction path. This occurs when a harmonic frequency becomes imaginary, and for the Raff surface this occurs for bends on both sides of the saddle point. Ab initio calculations can be helpful in determining if the bifurcation is an artifact of the form of the analytic potential function or if it is present in the actual system. When the MEP bifurcates it is probably best to base the RPH on a reference path centered on the ridge between two equivalent MEP's.[20,158] This requires extra effort when computing vibrational energy levels since the vibrational potential becomes a double-minimum one, but it probably reduces mode-mode coupling, which (see Sect. 2) is hard to treat accurately.

In making adjustments to the Raff surface we found that while we are indeed able to make localized changes, the changes caused by varying individual Sato parameters are not nearly as independent of each other as was the case[157] with the atom-diatom reaction $F + H_2$. To raise the saddle point to approximately the height of the PolCI one, all three Sato parameters need to be adjusted simultaneously in order to prevent other local maxima and minima from occurring.

An important consideration in the design of an analytic polyatomic PES is to know which region of the PES is most important for the dynamics. In VTST, an accurate PES is necessary only in the reaction swath. Thus, for the hybrid rate constants it is necessary to have an accurate representation of the potential along the MEP and for small deviations from it in the vicinity of dynamical bottlenecks, and for semiclassical tunneling calculations it is sometimes necessary to know the PES for larger deviations from the MEP along a lengthy segment of it. For VTST/κ calculations it is especially important that the frequencies as functions of s go smoothly and realistically from their reactant values to realistic saddle point values and then to their product values. This is an area where ab initio calculations can be very useful.

In Sect. 2 we discussed the practical advantages of valence coordinates for modelling anharmonicity. As discussed there, when the valence coordinates are non-redundant the valence-coordinate force field can be calculated directly from a global PES in any internal coordinate system,

e.g., interpair distances, as have been widely employed. Hase and coworkers[159-166] have made great progress, however, in modelling PES's directly in terms of valence coordinates. So far they have concentrated on association, dissociation, and isomerization reactions, but their methods could also be used, for example, in conjunction with MLEPS functions, for some of the interactions in atom-transfer reactions. The basic idea in all of Hase's valence-coordinate surfaces is to write the potential as a sum of Morse functions for all bonds, and harmonic, harmonic-quartic, or Taylor series potentials for all bends and torsions. The parameters in these terms are optimized using least-squares techniques with ab initio or spectroscopic input data.

Cobos and Troe[167] have demonstrated a strong sensitivity of the calculated rate constant for the dissociation of methane to a range parameter that they used to control the decay of the force constants involving the breaking bond to their asymptotic values. The same sensitivity to force constants can occur in atom-transfer reactions. Just as in the CH_4 dissociation, when an atom B is transferred between A and C, one must model the rate of decrease of an A-B-C bend potential as the AB or BC bond is broken. One of the first attempts to do this was by Johnston and Goldfinger.[168] They modelled the bending force constant by attenuating the equilibrium value according to the bond order of AB and BC. Sims and coworkers[169,170] have further tested the validity of this kind of model of the bending force constants for various hydrocarbons. They checked the effect of using both the square root of the product of the bond orders or the product of the bond orders when computing the force constants and then compared to experimental values. It was found that the product of the bond orders is the preferred choice if either of the bonds is undergoing a major change as the case would be during a chemical reaction. This suggests that some method of smoothly varying the bond order from 0 to 1 during the course of a reaction would be useful for modelling a bend potential on a polyatomic PES for VTST/κ calculations. Quack and Troe[123] used this same kind of idea in their statistical adiabatic channel model calculations of triatomic dissociation, for which they modelled the bond order as an exponential function of the deviation of the bond length from equilibrium. The exponential function they used contains an adjustable range parameter. More recently, however, Duchovic et al.,[166] in the course of designing a surface for the dissociation of methane, have performed ab initio calculations that indicate that the bending force constant may decay to zero more like a gaussian than an exponential.

Of course once one decides how to model the variation of a bending force constant with bond distance, this variation is easily incorporated into the PES if it is expressed in valence coordinates. As a final example of the flexibility of MLEPS functions, however, we point out that this can also be done by varying the Sato parameters in Raff's potential for CH_3 + HT. In particular we were able to adjust the C-H-T bend potential for a 40° deviation from collinearity to agree quite well with ab initio bend potentials for a 1.6 a_0 segment of the MEP by making one of the C-T triplet parameters a function of both the C-H-T bend angle and the H-T bond length. Although this procedure is mathematically quite different from the anti-Morse bend potential discussed in

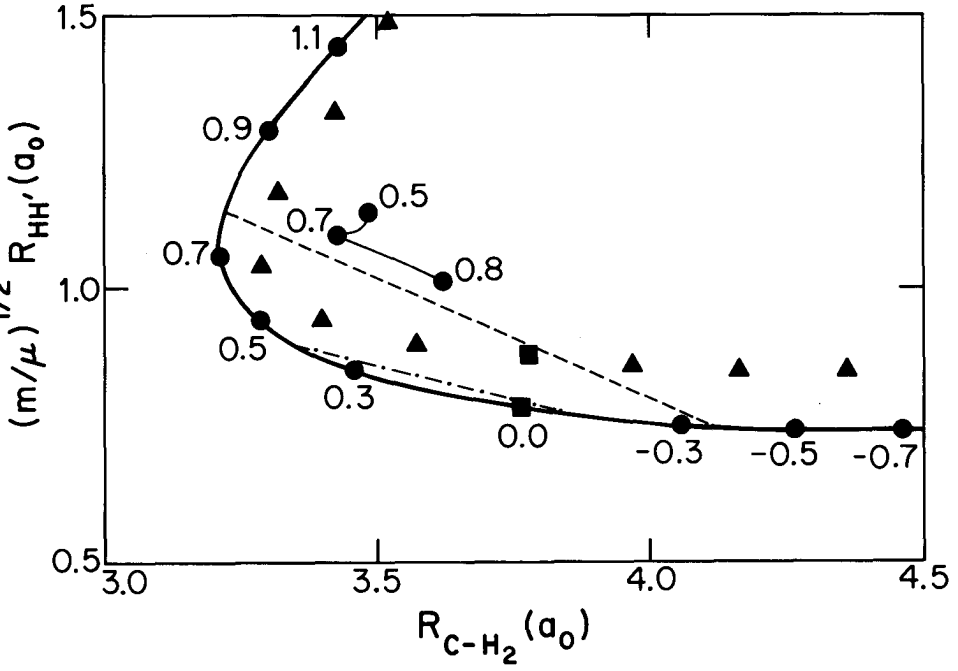

Fig. 3. Minimum-energy path and related quantities for $CH_3 + HH' \rightarrow CH_4 + H'$. All quantities for this figure are computed in the harmonic approximation for the vibrations. The abscissa is the distance from C to the center of mass of HH' and the ordinate is the scaled HH' distance, where the scale factor is $(m/\mu)^{\frac{1}{2}}$, $m = m_H/2$, and $\mu = m_{CH_3}m_{H_2}/m_{CH_5}$. The solid curve is the MEP, and the labels on it denote the values of the reaction coordinate s, where s is the distance along the MEP through mass-scaled coordinates with $\mu = m_{CH_3}m_{H_2}/m_{CH_5}$. The chain line and the dashed line are the ground-state LC3 tunneling paths for tunneling from one translational turning point of $V_a^G(s)$ to the other at the most probable tunneling energies (31.52 and 34.59 kcal/mol) at 350 and 250 K, respectively. The triangles denote coordinates of systems with zero amplitude in all their vibrational coordinates except the C-H-H' stretch, which is placed at the classical turning point on the concave side of the MEP. One of the points on the MEP and one of the triangles have been changed to squares to denote s=0. The other triangles are evenly spaced in s with interval $\Delta s = 0.2\ a_0$. The light curve connects the coordinates of systems with $s = 0.5\text{-}0.8\ a_0$ with zero amplitude in all vibrational coordinates except the C-H-H' stretch, which is placed at the radii of curvature for this mode.

Sect. 2, it is physically quite similar since the repulsive triplet C-T interaction potential in a C-H-T MLEPS function controls the bending potential for a C-H-T bend.

The final practical problem that we wish to emphasize in this chapter is the necessity to consider the whole reaction swath. We will use the PES of Raff for $CH_3 + HH'$ to illustrate how one may estimate the region over which the potential must be known. First of all we calculated the RPH for this system using the harmonic approximation and general methods presented elsewhere.[54] (This RPH is also discussed in Sect. 2.) At every point along the MEP, we calculated the C-H and H-H' bond lengths for the bonds being made and broken, and from them we calculated the Jacobi-like coordinates used as abscissa and ordinate in Fig. 3. The MEP is plotted as a solid curve in Fig. 3, which thereby becomes a two-dimensional internal-coordinate projection of the full-dimensional steepest descent path through mass-scaled coordinates. The distance s measured through the full set of mass-scaled coordinates along the MEP is shown at intervals of 0.2-0.3 a_0. Next, at every 0.2 a_0 along the MEP, we displaced the system through the full set of mass-scaled cartesian coordinates to the classical turning point (on the concave side

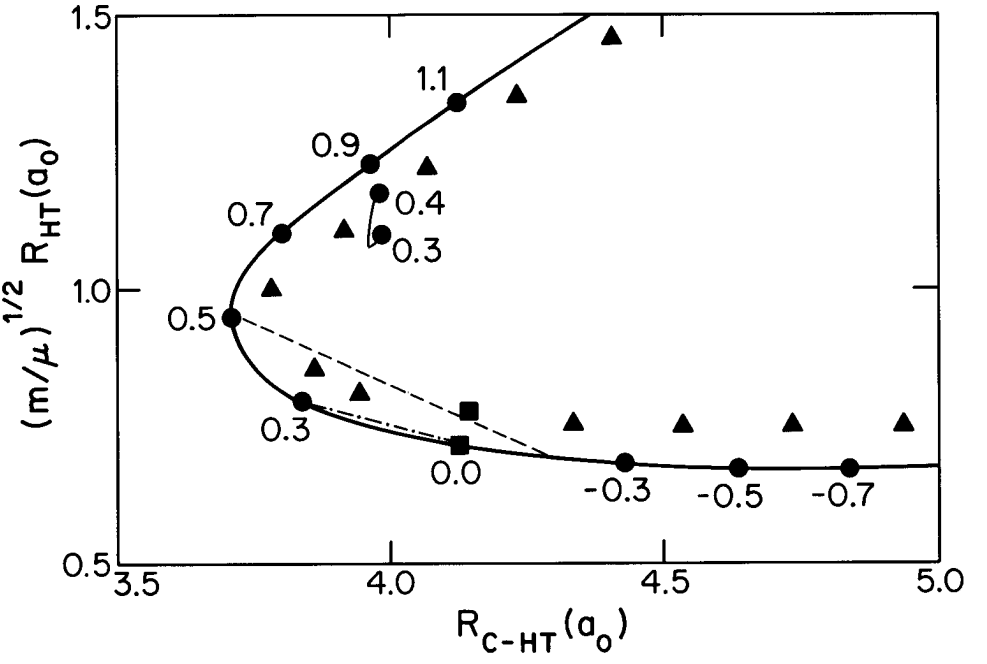

Fig. 4. Same as Fig. 3 except for $CH_3 + HT \rightarrow CH_4 + T$, $m = m_H m_T / m_{HT}$, $\mu = m_{CH_3} m_{HT} / m_{CH_4 T}$, the most probable tunneling energies are 32.07 and 34.40 kcal/mol, and the light curve is shown for $s = 0.3\text{-}0.4\ a_0$.

of the MEP) of the generalized normal mode corresponding to the bound C-H-H' motion. We calculated the ordinate and abscissa of Fig. 3 for these geometries and plotted these points as triangles. A curve (not shown explicitly) passing through these triangles is an analog of the Marcus-Coltrin tunneling path originally found[5,171] variationally for collinear H + H_2. The loci where the locally multivalued region of the reaction-path coordinate system, as estimated by the curvature of just the C-H-H' vibrational mode, gets closest to the MEP are shown in Fig. 3 as a short light curve. Two LC3 tunneling paths are also shown. In this case neither the analog of the Marcus-Coltrin path nor the LC3 tunneling paths reach into the region of locally multivalued coordinates, i.e., they are between the MEP and the light curve. Thus it appears sufficient to know the potential in regions where the RPH is valid. In Fig. 4 we give an analogous set of curves for CH_3 + HT → CH_4 + T, again using the Raff surface. The location where the boundary for the multivalued region gets closest to the MEP is shown between s = 0.3 and 0.4 a_0; again neither the analog of the Marcus-Coltrin path nor the LC3 tunneling paths enter the multivalued region. We conclude that an RPH formulation is adequate for CH_3 + H_2 → CH_4 + H and isotopic analogs, at least according to the Raff surface. A surface with a broader barrier would have more widely spread turning points, however, and for such a surface the LC3 path might enter the multivalued region. Furthermore, for other systems with much smaller skew angles, it becomes very likely that the tunneling paths will enter the multivalued region where the reaction-path coordinates break down. (Examples have been observed for atom-diatom collisions.[19-21]) In such cases, no RPH can be valid and we must consider a whole reaction swath, not just a local expansion about the MEP.

5. ACKNOWLEDGMENTS

The authors are grateful to several coworkers for work on various VTST projects. We would like to acknowledge Kenneth Dykema, Bruce C. Garrett, Mark S. Gordon, Nancy J. Kilpatrick, Alan W. Magnuson, John Overend, Sachchida N. Rai, Susan C. Tucker, and Trina Valencich for help with work discussed here or especially closely related to it. This work was supported in part by the U.S. Department of Energy, Office of Basic Energy Sciences, under contract no. DOE-AC02-79ER10425.

APPENDIX

In this appendix we give some examples of the coordinate transformation coefficients that appear in eqs. (40)-(43). For convenience we define $\bar{X}_{ij} = X_{ij}/r^{(0)}_{A_iA_j}$.

For the bond stretch $\Delta r_{AB} = r_{AB} - r^{(0)}_{AB}$, the coefficients can be obtained by differentiation of eq. (38) with respect to the difference cartesians X_{ij}. For $A_i = A_k = A_m = A$, $A_j = A_\ell = A_n = B$, and $\gamma_i \neq \gamma_k \neq \gamma_m$, this yields:[67]

$$\partial r_{AB}/\partial X_{ij} = \bar{X}_{ij} ,$$

$$\partial^2 r_{AB}/\partial X_{ij}^2 = (1 - \bar{X}_{ij}^2)/r_{AB}^{(0)} ,$$

$$\partial^2 r_{AB}/\partial X_{ij}\partial X_{k\ell} = -\bar{X}_{ij}\bar{X}_{k\ell}/r_{AB}^{(0)} ,$$

$$\partial^3 r_{AB}/\partial X_{ij}^3 = 3\bar{X}_{ij}(\bar{X}_{ij}^2 - 1)/(r_{AB}^{(0)})^2 ,$$

$$\partial^3 r_{AB}/\partial X_{ij}^2\partial X_{k\ell} = \bar{X}_{k\ell}(3\bar{X}_{ij}^2 - 1)/(r_{AB}^{(0)})^2 ,$$

$$\partial^3 r_{AB}/\partial X_{ij}\partial X_{k\ell}\partial X_{mn} = 3\bar{X}_{ij}\bar{X}_{k\ell}\bar{X}_{mn}/(r_{AB}^{(0)})^2 ,$$

$$\partial^4 r_{AB}/\partial X_{ij}^4 = -3(5\bar{X}_{ij}^4 - 6\bar{X}_{ij}^2 + 1)/(r_{AB}^{(0)})^3 ,$$

$$\partial^4 r_{AB}/\partial X_{ij}^3\partial X_{k\ell} = -3\bar{X}_{ij}\bar{X}_{k\ell}(5\bar{X}_{ij}^2 - 3)/(r_{AB}^{(0)})^3 ,$$

$$\partial^4 r_{AB}/\partial X_{ij}^2\partial X_{k\ell}^2 = (-15\bar{X}_{ij}^2\bar{X}_{k\ell}^2 + 3\bar{X}_{ij}^2 + 3\bar{X}_{k\ell}^2 - 1)/(r_{AB}^{(0)})^3 ,$$

and

$$\partial^4 r_{AB}/\partial X_{ij}^2\partial X_{k\ell}\partial X_{mn} = -3\bar{X}_{k\ell}\bar{X}_{mn}(5\bar{X}_{ij}^2 - 1)/(r_{AB}^{(0)})^3 .$$

For the angle deformation $\Delta\Phi_{ABC} = \Phi_{ABC} - \Phi_{ABC}^{(0)}$, we carry out a similar differentiation process with respect to eq. (39). For $A_i = A_k = A_m = A$, $A_j = A_\ell = A_n = A_{i'} = A_{k'} = B$, $A_{j'} = A_{\ell'} = C$, $C = \cos\Phi_{ABC}$, $S = \sin\Phi_{ABC}$, and $\gamma_i = \gamma_{i'} \neq \gamma_k = \gamma_{k'} \neq \gamma_m = \gamma_{m'}$, this yields:[67]

$$\partial\Phi_{ABC}/\partial X_{ij} = (C\bar{X}_{ij} - \bar{X}_{i'j'})/Sr_{AB}^{(0)} ,$$

$$\partial\Phi_{ABC}/\partial X_{i'j'} = (C\bar{X}_{i'j'} - \bar{X}_{ij})/Sr_{BC}^{(0)} ,$$

$$\partial^2\Phi_{ABC}/\partial X_{ij}^2 = [2\bar{X}_{ij}\bar{X}_{i'j'}/(r_{AB}^{(0)})^2 + C(1 - 3\bar{X}_{ij}^2) - C(\partial\Phi_{ABC}/\partial X_{ij})^2]/S ,$$

$$\partial^2\Phi_{ABC}/\partial X_{ij}\partial X_{k\ell} = [(\bar{X}_{ij}\bar{X}_{k'\ell'} + i'j'k\ell - 3\bar{X}_{ij}\bar{X}_{k\ell}C)/(r_{AB}^{(0)})^2 - C(\partial\Phi_{ABC}/\partial X_{ij})(k\ell)]/S ,$$

$$\partial^2\Phi_{ABC}/\partial X_{ij}\partial X_{i'j'} = [(\bar{X}_{ij}^2 + i'j' - \bar{X}_{ij}\bar{X}_{i'j'}C - 1)/r_{AB}^{(0)}r_{BC}^{(0)} - C(\partial\Phi_{ABC}/\partial X_{ij})(i'j')]/S \quad ,$$

$$\partial^2\Phi_{ABC}/\partial X_{ij}\partial X_{k'\ell'} = [(\bar{X}_{ij}\bar{X}_{k\ell} + i'j'k'\ell' - \bar{X}_{ij}\bar{X}_{k'\ell'}C)/r_{AB}^{(0)}r_{BC}^{(0)} - C(\partial\Phi_{ABC}/\partial X_{ij})(k'\ell')]/S \quad ,$$

$$\partial^3\Phi_{ABC}/\partial X_{ij}^3 = 3[\bar{X}_{i'j'} - 3\bar{X}_{ij}(C + \bar{X}_{ij}\bar{X}_{i'j'}) + 5C\bar{X}_{ij}^3]/S(r_{AB}^{(0)})^3 + (\partial\Phi_{ABC}/\partial X_{ij})^3 - 3C(\partial\Phi_{ABC}/\partial X_{ij})(\partial^2\Phi_{ABC}/\partial X_{ij}^2)/S \quad ,$$

$$\partial^3\Phi_{ABC}/\partial X_{ij}^2\partial X_{k\ell} = \{\bar{X}_{k'\ell'} - 3[C\bar{X}_{k\ell} + 2\bar{X}_{ij}\bar{X}_{i'j'}\bar{X}_{k\ell} + \bar{X}_{ij}^2 \times (\bar{X}_{k'\ell'} - 5C\bar{X}_{k\ell})]\}/S(r_{AB}^{(0)})^3 - C[2(\partial\Phi_{ABC}/\partial X_{ij}) \times (\partial^2\Phi_{ABC}/\partial X_{ij}\partial X_{k\ell}) + (\partial\Phi_{ABC}/\partial X_{k\ell})(\partial^2\Phi_{ABC}/\partial X_{ij}^2)]/S + (\partial\Phi_{ABC}/\partial X_{ij})^2(\partial\Phi_{ABC}/\partial X_{k\ell}) \quad ,$$

$$\partial^3\Phi_{ABC}/\partial X_{ij}\partial X_{k\ell}\partial X_{mn} = 3[5C\bar{X}_{ij}\bar{X}_{k\ell}\bar{X}_{mn} - (\bar{X}_{i'j'}\bar{X}_{k\ell}\bar{X}_{mn} + ijk'\ell'mn + ijk\ell m'n')]/S(r_{AB}^{(0)})^3 - C[(\partial\Phi_{ABC}/\partial X_{ij})(\partial^2\Phi_{ABC}/\partial X_{k\ell}\partial X_{mn}) + k\ell ijmn + mnijk\ell]/S + (\partial\Phi_{ABC}/\partial X_{ij})(k\ell)(mn) \quad ,$$

$$\partial^3\Phi_{ABC}/\partial X_{ij}^2\partial X_{i'j'} = [3\bar{X}_{ij}(1 - \bar{X}_{ij}^2 + C\bar{X}_{ij}\bar{X}_{i'j'}) - 2\bar{X}_{ij}\bar{X}_{i'j'}^2 - C\bar{X}_{i'j'}]/S(r_{AB}^{(0)})^2r_{BC}^{(0)} - 2C[(\partial\Phi_{ABC}/\partial X_{ij})(\partial^2\Phi_{ABC}/\partial X_{ij}\partial X_{i'j'}) + i'j'ijij]/S + (\partial\Phi_{ABC}/\partial X_{ij})^2(\partial\Phi_{ABC}/\partial X_{i'j'}) \quad ,$$

$$\partial^3\Phi_{ABC}/\partial X_{ij}^2\partial X_{k'\ell'} = [\bar{X}_{k\ell} - 2\bar{X}_{ij}\bar{X}_{i'j'}\bar{X}_{k'\ell'} - C\bar{X}_{k'\ell'} + 3\bar{X}_{ij}^2(C\bar{X}_{k'\ell'} - \bar{X}_{k\ell})]/S(r_{AB}^{(0)})^2r_{BC}^{(0)} - 2C[(\partial\Phi_{ABC}/\partial X_{ij}) \times (\partial^2\Phi_{ABC}/\partial X_{ij}\partial X_{k'\ell'}) + k'\ell'ijij]/S +$$

$$+ (\partial\Phi_{ABC}/\partial X_{ij})^2(\partial\Phi_{ABC}/\partial X_{k'\ell'}) ,$$

$$\partial^3\Phi_{ABC}/\partial X_{ij}\partial X_{k\ell}\partial X_{i'j'} = [\bar{X}_{k\ell}(1 - 3\bar{X}_{ij}^2 + 3\mathcal{C}\bar{X}_{ij}\bar{X}_{i'j'}) - \bar{X}_{i'j'} \times$$

$$\times (\bar{X}_{i'j'}\bar{X}_{k\ell} + ijk'\ell')]/\mathcal{S}(r_{AB}^{(0)})^2 r_{BC}^{(0)} - \mathcal{C}[(\partial\Phi_{ABC}/\partial X_{ij}) \times$$

$$\times (\partial^2\Phi_{ABC}/\partial X_{k\ell}\partial X_{i'j'}) + k\ell iji'j' + i'j'ijk\ell]/\mathcal{S} +$$

$$+ (\partial\Phi_{ABC}/\partial X_{ij})(k\ell)(i'j') ,$$

$$\partial^3\Phi_{ABC}/\partial X_{ij}\partial X_{k\ell}\partial X_{m'n'} = -[\bar{X}_{m'n'}(\bar{X}_{i'j'}\bar{X}_{k\ell} + k'\ell'ij) + 3\bar{X}_{ij}\bar{X}_{k\ell} \times$$

$$\times (\bar{X}_{mn} - \mathcal{C}\bar{X}_{m'n'})]/\mathcal{S}(r_{AB}^{(0)})^2 r_{BC}^{(0)} - \mathcal{C}[(\partial\Phi_{ABC}/\partial X_{ij}) \times$$

$$\times (\partial^2\Phi_{ABC}/\partial X_{k\ell}\partial X_{m'n'}) + k\ell ijm'n' + m'n'ijk\ell]/\mathcal{S} +$$

$$+ (\partial\Phi_{ABC}/\partial X_{ij})(k\ell)(m'n') ,$$

and so on for the higher derivatives. In writing these expressions we used the convention that if a term or factor is identical to the previous one except for the lower case subscripts, we only repeat those. Because of the $\mathcal{S}^{-1}$ factors in these equations they cannot be used for a linear angle. One possible set of modifications that is useful in such a case is described in Ref. 67. Similar equations to those given above but for out-of-plane bending and torsional angle internal coordinates are given elsewhere.[74,78]

REFERENCES

1. Potential Energy Surfaces and Dynamics Calculations, edited by D.G. Truhlar (Plenum, New York, 1981).
2. J.N. Murrell, S. Carter, S.C. Farantos, P. Huxley, and A.J.C. Varandas, Molecular Potential Energy Functions (John Wiley and Sons, Chichester, 1984).
3. Dynamics of Molecular Collisions, Part B, edited by W.H. Miller (Plenum, New York, 1976).
4. D.G. Truhlar, F.B. Brown, D.W. Schwenke, R. Steckler, and B.C. Garrett, in Comparison of Ab Initio Quantum Chemistry with Experiment, edited by R.J. Bartlett (D. Reidel, Dordrecht, Holland), in press.
5. R.A. Marcus, J. Phys. Chem. 83, 204 (1979).
6. K. Fukui, Acc. Chem. Res. 14, 363 (1981).
7. K. Morokuma and S. Kato, in Potential Energy Surfaces and Dynamics Calculations, edited by D.G. Truhlar (Plenum, New York, 1981), p. 243.
8. W.H. Miller, J. Phys. Chem. 87, 3811 (1983).
9. D.G. Truhlar and B.C. Garrett, Acc. Chem. Res. 13, 440 (1980).

10. D.G. Truhlar, A.D. Isaacson, R.T. Skodje, and B.C. Garrett, J. Phys. Chem. 86, 2252 (1982), 87, 4554E (1983).
11. D.G. Truhlar and B.C. Garrett, Annu. Rev. Phys. Chem. 35, 159 (1984).
12. D.G. Truhlar and A.D. Isaacson, J. Chem. Phys. 77, 3516 (1982).
13. D.C. Clary, B.C. Garrett, and D.G. Truhlar, J. Chem. Phys. 78, 777 (1983).
14. D.G. Truhlar, W.L. Hase, and J.T. Hynes, J. Phys. Chem. 87, 2664, 5523E (1983).
15. B.C. Garrett and D.G. Truhlar, J. Chem. Phys. 81, 309 (1984).
16. D.G. Truhlar, B.C. Garrett, P.G. Hipes, and A. Kuppermann, J. Chem. Phys. 81, 3542 (1984).
17. A.D. Isaacson, M.T. Sund, S.N. Rai, and D.G. Truhlar, J. Chem. Phys. 82, 1338 (1985).
18. B.C. Garrett and D.G. Truhlar, J. Phys. Chem. 89, 2204 (1985).
19. B.C. Garrett, N. Abusalbi, D.J. Kouri, and D.G. Truhlar, J. Chem. Phys. 83, in press.
20. B.C. Garrett, D.G. Truhlar, A.F. Wagner, and T.H. Dunning, Jr., J. Chem. Phys. 78, 4400 (1983).
21. D.K. Bondi, J.N.L. Connor, B.C. Garrett, and D.G. Truhlar, J. Chem. Phys. 78, 5981 (1983).
22. B.C. Garrett and D.G. Truhlar, J. Chem. Phys. 79, 4931 (1983).
23. R. Steckler, D.G. Truhlar, B.C. Garrett, N.C. Blais, and R.B. Walker, J. Chem. Phys. 81, 5700 (1984).
24. F.B. Brown, R. Steckler, D.W. Schwenke, D.G. Truhlar, and B.C. Garrett, J. Chem. Phys. 82, 188 (1985).
25. B.C. Garrett and D.G. Truhlar, J. Phys. Chem. 86, 1136 (1982), 87, 4554E (1983).
26. B.C. Garrett, D.G. Truhlar, R.S. Grev, G.C. Schatz, and R.B. Walker, J. Phys. Chem. 85, 3806 (1981).
27. R.T. Skodje, D.W. Schwenke, D.G. Truhlar, and B.C. Garrett, J. Phys. Chem. 88, 628 (1984).
28. R.T. Skodje, D.W. Schwenke, D.G. Truhlar, and B.C. Garrett, J. Chem. Phys. 80, 3569 (1984).
29. B.C. Garrett, D.W. Schwenke, R.T. Skodje, D. Thirumalai, T.C. Thompson, and D.G. Truhlar, in Resonances, edited by D.G. Truhlar (American Chemical Society, Washington, 1984), p. 375.
30. F.B. Brown, S.C. Tucker, and D.G. Truhlar, J. Chem. Phys. 83, in press.
31. W.H. Miller and S.-H. Shi, J. Chem. Phys. 75, 2258 (1981).
32. C.J. Cerjan, S. Shi, and W.H. Miller, J. Phys. Chem. 86, 2244 (1982).
33. K. Morokuma, S. Kato, K. Kitaura, S. Obara, K. Ohta, and M. Hanamura, in New Horizons of Quantum Chemistry, edited by P.-O. Lowdin and B. Pullman (D. Reidel, Dordrecht, Holland, 1983), p. 221.
34. W.H. Miller, N.C. Handy, and J.E. Adams, J. Chem. Phys. 72, 99 (1980).
35. G. Natanson, Mol. Phys. 46, 481 (1982).
36. D.G. Truhlar, Int. J. Quantum Chem. Symp. 17, 77 (1983).
37. G.L. Hofacker, Z. Naturforsch. A 18, 607 (1963).
38. R.A. Marcus, J. Chem. Phys. 45, 4493, 4500 (1966).

39. D.G. Truhlar, J. Chem. Phys. 53, 2041 (1970).
40. K. Fukui, A. Tachibana, and K. Yamashita, Int. J. Quantum Chem. Symp. 15, 621 (1981).
41. A. Tweedale and K.J. Laidler, J. Chem. Phys. 53, 2045 (1970).
42. B.C. Garrett and D.G. Truhlar, J. Phys. Chem. 83, 1079 (1979), 84, 682E (1980), 87, 4553E (1983).
43. B.C. Garrett and D.G. Truhlar, J. Amer. Chem. Soc. 101, 4534 (1979).
44. B.C. Garrett, D.G. Truhlar, R.S. Grev, and A.W. Magnuson, J. Phys. Chem. 84, 1730 (1980), 87, 4554E (1983).
45. S. Glasstone, K.J. Laidler, and H. Eyring, Theory of Rate Processes (McGraw-Hill, New York, 1941).
46. J.C. Keck, Adv. Chem. Phys. 13, 85 (1967).
47. I. Shavitt, Theoretical Chemistry Laboratory Report WIS-AEC-23, University of Wisconsin, 11 August 1959 (unpublished).
48. D.G. Truhlar and A. Kuppermann, J. Amer. Chem. Soc. 93, 1840 (1971).
49. K. Fukui, S. Kato, and H. Fujimoto, J. Amer. Chem. Soc. 97, 1 (1975).
50. H.F. Schaefer III, Chem. Brit. 11, 227 (1975).
51. B.C. Garrett and D.G. Truhlar, J. Phys. Chem. 83, 1052, 3058E (1979), 87, 4553E (1983).
52. R.T. Skodje, D.G. Truhlar, and B.C. Garrett, J. Phys. Chem. 85, 3019 (1981).
53. R.T. Skodje, D.G. Truhlar, and B.C. Garrett, J. Chem. Phys. 77, 5955 (1982).
54. D.G. Truhlar, A.D. Isaacson, and B.C. Garrett, in The Theory of Chemical Reaction Dynamics, edited by M. Baer (CRC Press, Boca Raton, FL, 1985), Vol. 4, p. 1.
55. V.K. Babamov and R.A. Marcus, J. Chem. Phys. 74, 1790 (1978).
56. P. Pechukas and F.J. McLafferty, J. Chem. Phys. 58, 1622 (1973).
57. B.C. Garrett and D.G. Truhlar, J. Phys. Chem. 83, 1915 (1979).
58. B.C. Garrett and D.G. Truhlar, J. Amer. Chem. Soc. 101, 5207 (1979).
59. A.D. Isaacson and D.G. Truhlar, J. Chem. Phys. 76, 1380 (1982).
60. G.C. Schatz and H. Elgersma, Chem. Phys. Lett. 73, 21 (1980).
61. S.P. Walch and T.H. Dunning, J. Chem. Phys. 72, 1303 (1980).
62. W.B. Wilson, Jr., J.C. Decius, and P.C. Cross, Molecular Vibrations (McGraw-Hill, New York, 1955), p. 19, (a) p. 172.
63. D.G. Truhlar, J. Mol. Spectrosc. 38, 415 (1971).
64. A.D. Isaacson, D.G. Truhlar, K. Scanlon, and J. Overend, J. Chem. Phys. 75, 3017 (1981).
65. B.C. Garrett and D.G. Truhlar, J. Chem. Phys. 72, 3460 (1980).
66. H.H. Nielsen, Encycl. Phys. 37/part one, 173 (1959).
67. M.A. Pariseau, I. Suzuki, and J. Overend, J. Chem. Phys. 42, 2335 (1965).
68. D.G. Truhlar, R.W. Olson, A.C. Jeannotte, and J. Overend, J. Amer. Chem. Soc. 98, 2373 (1976).
69. D. Papousek and M.R. Aliev, Molecular Vibrational-Rotational Spectra (Elsevier, Amsterdam, 1982), p. 38.
70. B.C. Garrett, D.G. Truhlar, and A.W. Magnuson, J. Chem. Phys. 76, 2321 (1982).
71. H.S. Johnston and C.A. Parr, J. Amer. Chem. Soc. 85, 2544 (1963).

72. A.R. Hoy, I.M. Mills, and G. Strey, Mol. Phys. 24, 1265 (1972).
73. M.A. Pariseau, I. Suzuki, and J. Overend, J. Chem. Phys. 44, 3561 (1966).
74. S. Califano, Vibrational States (Wiley, London, 1976).
75. B. Crawford, Jr. and J. Overend, J. Mol. Spectrosc. 12, 307 (1964).
76. W.B. Brown and E. Steiner, J. Mol. Spectrosc. 10, 348 (1963).
77. S. Brodersen and J. Christoffersen, J. Mol. Spectrosc. 12, 303 (1964).
78. K. Machida, J. Chem. Phys. 44, 4186 (1966).
79. I. Suzuki and J. Overend. Spectrochim. Acta 3, 1093 (1981).
80. N.W. Bazley and D.W. Fox, Phys. Rev. 124, 483 (1961).
81. K.S. Pitzer and W.D. Gwinn, J. Chem. Phys. 10, 428 (1942).
82. A.D. Isaacson and D.G. Truhlar, J. Chem. Phys. 75, 4090 (1981).
83. D.A. McQuarrie, Statistical Mechanics (Harper and Row, New York, 1976).
84. D.L. Bunker, J. Chem. Phys. 37, 393 (1962).
85. W.L. Hase and D.G. Buckowski, Chem. Phys. Lett. 74, 284 (1980).
86. J.E. Adams and J.D. Doll, J. Chem. Phys. 74, 5332 (1981).
87. A.E. Barton and B.J. Howard, Faraday Discuss. Chem. Soc. 73, 45 (1982).
88. A.F. Voter, J. Chem. Phys. 82, 1890 (1985).
89. D.L. Freeman and J.D. Doll, J. Chem. Phys. 80, 5709 (1984).
90. P. Pulay, Mol. Phys. 17, 197 (1969).
91. P. Pulay, in Applications of Electronic Structure Theory, edited by H.F. Schaefer (Plenum, New York, 1977), p. 153.
92. P. Pulay, in The Force Concept in Chemistry, edited by B.M. Deb (Van Nostrand Reinhold, New York, 1981), p. 449.
93. J.A. Pople, R. Krishnan, H.B. Schlegel, and J.B. Binkley, Int. J. Quantum Chem. Symp. 13, 225 (1979).
94. J.D. Goddard, N.C. Handy, and H.F. Schaefer, J. Chem. Phys. 71, 1525 (1979).
95. S. Kato and K. Morokuma, Chem. Phys. Lett. 65, 19 (1979).
96. B.R. Brooks, W.D. Laidig, P. Saxe, J.D. Goddard, Y. Yamaguchi, and H.F. Schaefer, J. Chem. Phys. 72, 4652 (1980).
97. R. Krishnan, H.B. Schlegel, and J.A. Pople, J. Chem. Phys. 72, 4654 (1980).
98. Y. Osamura, Y. Yamaguchi, and H.F. Schaefer, J. Chem. Phys. 77, 383 (1982).
99. M. Page, P. Saxe, G.F. Adams, and B.H. Lengsfield, J. Chem. Phys. 81, 434 (1984).
100. G. Fitzgerald, R. Harrison, W.D. Laidig, and R.J. Bartlett, J. Chem. Phys. 82, 4379 (1985).
101. J.W. McIver, Jr. and A. Komornicki, Chem. Phys. Lett. 10, 303 (1971).
102. D. Poppinger, Chem. Phys. Lett. 34, 332 (1975).
103. D. Poppinger, Chem. Phys. Lett. 35, 550 (1975).
104. A. Komornicki, K. Ishida, K. Morokuma, R. Ditchfield, and M. Conrad, Chem. Phys. Lett. 45, 595 (1977).
105. B. Schlegel, J. Comput. Chem. 3, 214 (1982).
106. A. Banerjee, N. Adams, J. Simons, and R. Shepard, J. Phys. Chem. 89, 52 (1985).

107. Y. Osamura, Y. Yamaguchi, P. Saxe, M.A. Vincent, J.F. Gaw, and H.F. Schaefer, Chem. Phys. 72, 131 (1982).
108. Y. Yamaguchi, Y. Osamura, G. Fitzgerald, and H.F. Schaefer, J. Chem. Phys. 78, 1607 (1983).
109. R.N. Camp, H.F. King, J.W. McIver, Jr., and D. Mullally, J. Chem. Phys. 79, 1088 (1983).
110. D.J. Fox, Y. Osamura, M.R. Hoffman, J.F. Gaw, G. Fitzgerald, Y. Yamaguchi, and H.F. Schaefer, Chem. Phys. Lett. 102, 17 (1983).
111. M.R. Hoffman, D.J. Fox, J.F. Gaw, Y. Osamura, Y. Yamaguchi, R.S. Grev, G. Fitzgerald, H.F. Schaefer, P.J. Knowles, and N.C. Handy, J. Chem. Phys. 80, 2660 (1984).
112. P. Pulay, J. Chem. Phys. 78, 5043 (1983).
113. P. Jørgensen and J. Simons, J. Chem. Phys. 79, 334 (1983).
114. J.F. Gaw, Y. Yamaguchi, and H.F. Schaefer, J. Chem. Phys. 81, 6395 (1984).
115. S. Kato, H. Kato, and H. Fukui, J. Amer. Chem. Soc. 99, 684 (1977).
116. S.K. Gray, W.H. Miller, Y. Yamaguchi, and H.F. Schaefer, J. Chem. Phys. 73, 2733 (1980).
117. K. Yamashita and Y. Yamabe, Int. J. Quantum Chem. Symp. 17, 177 (1983).
118. S.M. Colwell and N.C. Handy, J. Chem. Phys. 82, 1281 (1985).
119. A. Tachibana, T. Okazaki, M. Koizumi, K. Hori, and T. Yamabe, J. Amer. Chem. Soc. 107, 1190 (1985).
120. D.G. Truhlar, N.J. Kilpatrick, and B.C. Garrett, J. Chem. Phys. 78, 2438 (1983).
121. H.S. Johnston and J. Heicklen, J. Phys. Chem. 66, 532 (1962).
122. B.C. Garrett and D.G. Truhlar, J. Phys. Chem. 83, 2921 (1979).
123. M. Quack and J. Troe, Ber. Bunsenges. Phys. Chem. 78, 240 (1974).
124. M. Quack and J. Troe, Ber. Bunsenges. Phys. Chem. 79, 170, 469 (1975).
125. D.G. Truhlar and A. Kuppermann, J. Chem. Phys. 52, 2232 (1970).
126. M.J. Stern, A. Persky, and F.S. Klein, J. Chem. Phys. 58, 5697 (1973).
127. J.T. Muckerman, Theor. Chem. Adv. Perspect. A 6, 1 (1981).
128. J.W. Duff and D.G. Truhlar, J. Chem. Phys. 62, 2477 (1975).
129. T. Carrington, Jr., L.M. Hubbard, H.F. Schaefer III, and W.H. Miller, J. Chem. Phys. 80, 4347 (1984).
130. M.V. Basilevsky and V.M. Ryaboy, Chem. Phys. 41, 461 (1979).
131. B.C. Garrett, R.T. Skodje, and D.G. Truhlar, unpublished calculations.
132. L.M. Raff, J. Chem. Phys. 60, 2220 (1974).
133. T. Valencich and D.L. Bunker, J. Chem. Phys. 61, 21 (1974).
134. S. Chapman and D.L. Bunker, J. Chem. Phys. 62, 2890 (1975).
135. W.A. Lathan, W.J. Hehre, L.A. Curtiss, and J.A. Pople, J. Amer. Chem. Soc. 93, 6377 (1971).
136. S. Ehrenson and M.D. Newton, Chem. Phys. Lett. 13, 24 (1972).
137. K. Morokuma and R.E. Davis, J. Amer. Chem. Soc. 94, 1060 (1972).
138. K. Fukui, S. Kato, and H. Fujimoto, J. Amer. Chem. Soc. 97, 1 (1975).

139. K. Niblaeus, B.O. Roos,and P.E.M. Siegbahn, Chem. Phys. 26, 59 (1977).
140. P. Cársky and R. Zahradnik, J. Mol. Struct. 54, 247 (1979).
141. P. Cársky and R. Zahradnik, Int. J. Quantum Chem. 16, 243 (1979).
142. P. Cársky, Coll. Czech. Chem. Comm. 44, 3452 (1979).
143. S.P. Walch, J. Chem. Phys. 72, 4932 (1980).
144. G.C. Schatz, S.P. Walch, and A.F. Wagner, J. Chem. Phys. 73, 4536 (1980).
145. G.C. Schatz, A.F. Wagner, and T.H. Dunning, Jr., J. Phys. Chem. 88, 221 (1984).
146. M.S. Gordon, D.R. Gano, and J.A. Boatz, J. Amer. Chem. Soc. 105, 5771 (1983).
147. S. Sana, G. Leroy, and J.L. Villaveces, Theoret. Chim. Acta 65, 109 (1984).
148. B. Maessen, P. Bopp, D.R. McLaughlin, and M. Wolfsberg, Z. Naturfor. 39a, 1005 (1984).
149. M.W. Schmidt, M.S. Gordon, and M. Dupuis, J. Amer. Chem. Soc. 107, 2585 (1985).
150. K. Ishida, K. Morokuma, and A. Komornicki, J. Chem. Phys. 66, 2153 (1977).
151. S.M. Colwell, Mol. Phys. 51, 1217 (1984).
152. D.G. Truhlar and C.J. Horowitz, J. Chem. Phys. 68, 2466 (1978), 71, 1514E (1979).
153. M. Dupuis, D. Spangler, and J.J. Wendoloski, Program QG01, in NRCC Software Catalog (Lawrence Berkeley Laboratory technical report LBL-10811, Berkeley, CA, 1980), p. 60.
154. P.J. Kuntz, E.M. Nemeth, J.C. Polanyi, S.D. Rosner, and C.E. Young, J. Phys. Chem. 44, 1168 (1966).
155. C.A. Parr and D.G. Truhlar, J. Phys. Chem. 75, 1844 (1971).
156. N.C. Blais and D.G. Truhlar, J. Chem. Phys. 58, 4186 (1974), 65, 3803E (1976).
157. F.B. Brown, R. Steckler, D.W. Schwenke, D.G. Truhlar, and B.C. Garrett, J. Chem. Phys. 82, 188 (1985).
158. W.H. Miller, J. Phys. Chem. 87, 21 (1983).
159. D.L. Bunker and W.L. Hase, J. Chem. Phys. 59, 4621 (1973), 69, 4711E (1978).
160. W.L. Hase, G. Mrowka, R.J. Brudzynski, and C.S. Sloane, J. Chem. Phys. 69, 3548 (1978).
161. W.L. Hase, D.M. Ludlow, R.J. Wolf, and T. Schlick, J. Phys. Chem. 85, 958 (1981).
162. E.R. Grant and D.L. Bunker, J. Chem. Phys. 68, 628 (1978).
163. C.S. Sloane and W.L. Hase, Discuss. Faraday Soc. 62, 210 (1977).
164. P.J. Nagy and W.L. Hase, Chem. Phys. Lett. 54, 73 (1978).
165. W.L. Hase and K.C. Bhalla, J. Chem. Phys. 75, 2807 (1981).
166. R.J. Duchovic, W.L. Hase, and H.B. Schlegel, J. Phys. Chem. 88, 1339 (1984).
167. C.J. Cobos and J. Troe, Chem. Phys. Lett. 113, 41 (1985).
168. H.S. Johnston and P. Goldfinger, J. Chem. Phys. 37, 700 (1962).
169. G.W. Burton, L.B. Sims, J.C. Wilson, and A. Fry, J. Amer. Chem. Soc. 99, 3371 (1977).
170. L.B. Sims and D.E. Lewis, Isotopes in Organic Chemistry, Vol. 6,

"Isotopic Effects: Recent Developments in Theory and Experiment", edited by E. Buncel and C.C. Lee (Elsevier, Amsterdam, 1984), p. 161.

171. R.A. Marcus and M.E. Coltrin, J. Chem. Phys. 67, 2609 (1977).